nature protocols

https://doi.org/10.1038/s41596-024-01097-6

Protocol

Check for updates

Pair correlation microscopy of intracellular molecular transport

Julissa Sanchez-Velasquez[1], Ashleigh Solano[1], Michelle A. Digman[2], Enrico Gratton[2], Francesco Cardarelli[3] & Elizabeth Hinde[1]

Abstract

Pair correlation microscopy is a unique approach to fluorescence correlation spectroscopy that can track the long-range diffusive route of a population of fluorescent molecules in live cells with respect to intracellular architecture. This method is based on the use of a pair correlation function (pCF) that, through spatiotemporal comparison of fluctuations in fluorescence intensity recorded throughout a microscope data acquisition, enables changes in a molecule's arrival time to be spatially mapped and statistically quantified. In this protocol, we present guidelines for the measurement and analysis of line scan pair correlation microscopy data acquired on a confocal laser scanning microscope (CLSM), which will enable users to extract a fluorescent molecule's transport pattern throughout a living cell, and then quantify the molecular accessibility of intracellular barriers encountered or the mode of diffusion governing a molecular trafficking event. Finally, we demonstrate how this protocol can be extended to a two-channel line scan acquisition that, when coupled with a cross pCF calculation, enables a fluorescent molecule's transport pattern to be selectively tracked as a function of complex formation with a spectrally distinct fluorescent ligand. For a skilled user of a CLSM, the line scan data acquisition and analysis described in this protocol will take ~1–2 d, depending on the sample and the number of experiments to be processed.

Key points

- This protocol describes a method for tracking fluorescent molecule transport throughout a living cell that is based on pair correlation function analysis of fluctuations in fluorescence intensity acquired throughout a microscope data acquisition.
- This protocol builds on previous approaches to fluorescence correlation spectroscopy by introducing a spatial component during data analysis that allows the impact of intracellular barriers on diffusion to be calculated.

Key references

Digman, M. A. & Gratton, E. *Biophys. J.* **97**, 665–673 (2009): https://doi.org/10.1016/j.bpj.2009.04.048

Hinde, E. et al. *Nat. Nanotechnol.* **12**, 81–89 (2017): https://doi.org/10.1038/nnano.2016.160

Hinde, E. et al. *Proc. Natl Acad. Sci. USA* **107**, 16560–16565 (2010): https://doi.org/10.1073/pnas.1006731107

Cardarelli, F. & Gratton, E. *PLoS One* **5**, e10475 (2010): https://doi.org/10.1371/journal.pone.0010475

[1]School of Physics, Faculty of Science, University of Melbourne, Melbourne, Australia. [2]Laboratory of Fluorescence Dynamics, The Henry Samueli School of Engineering, University of California, Irvine, CA, USA. [3]Scuola Normale Superiore, Laboratorio NEST, Pisa, Italy. e-mail: elizabeth.hinde@unimelb.edu.au

Introduction

Understanding the molecular mechanisms that underlie intracellular signal transmission requires microscopy methods that can track molecular transport throughout a living cell. Here, we present a protocol for a fluorescence fluctuation-based method called pair correlation microscopy, which can quantitatively map the diffusive route of a population of fluorescent molecules with respect to live cell architecture[1]. Pair correlation microscopy is centered around a pair correlation function (pCF) that temporally compares spatially distinct fluctuations in fluorescent protein intensity recorded throughout a microscope data acquisition (line or frame)[2,3] (Fig. 1a) to derive a matrix of pCF profiles that report the spatiotemporal evolution of molecular transport throughout a cell (Fig. 1b) and changes in the arrival time of a molecular trafficking event with respect to intracellular barriers of interest (e.g., the nuclear pore complex)[1,4,5] (Fig. 1c).

To date, the unique capacity of pair correlation microscopy to probe the molecular accessibility of the intracellular landscape has been limited by the complexity of data analysis. Therefore, in this protocol, we provide a step-by-step workflow for the measurement and analysis of line-scan pair correlation microscopy data acquired on a confocal laser scanning microscope (CLSM) in a living cell. We incorporate a fit-based strategy for the quantification of pCF profiles that greatly enhances usability and has the potential to be easily adapted to a CLSM frame scan acquisition through the use of a radial pCF—a 2D pCF that radially correlates a central fluorescence fluctuation with surrounding fluctuations positioned at a fixed distance[3,6]. In particular, this line scan pair correlation microscopy workflow will enable users to translate a fluorescent molecule's intracellular transport pattern into a series of arrival times associated with molecule numbers, which can then be used to calculate the efficiency[5], directionality[4] and mode of diffusion[7] that underpins molecular movement between subcellular compartments (e.g., the cytoplasm and nucleus)[8–10] as well as with respect to intracellular structures (e.g., actin and chromatin)[11–17]. Importantly, we also demonstrate how to extend this line scan pair correlation microscopy workflow to a two-channel acquisition that, when coupled with a cross-pCF calculation, enables a fluorescent molecule's transport pattern to be selectively

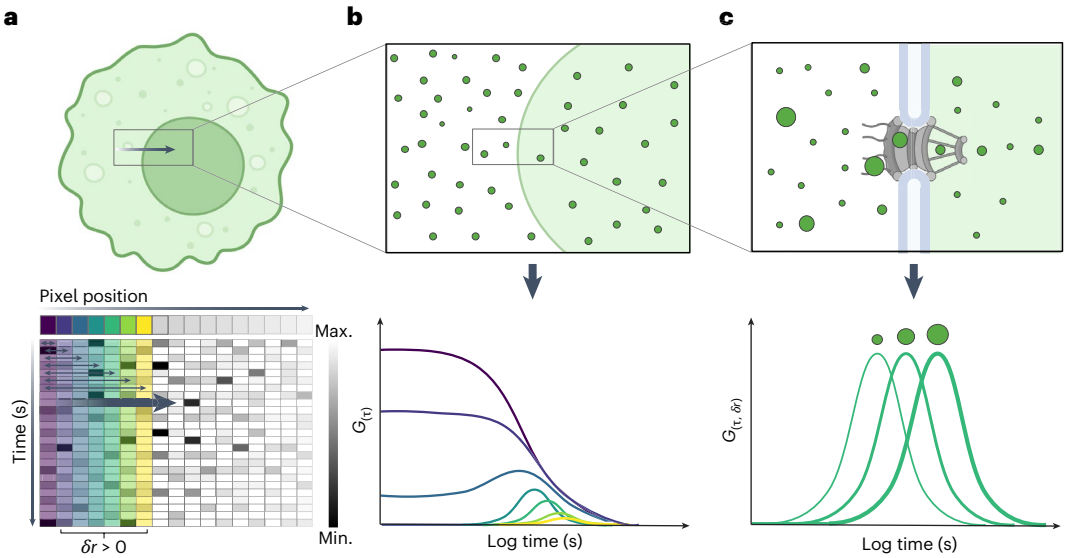

Fig. 1 | Schematic diagram of the pCF principle. a, pCF analysis involves spatial comparison of temporal fluctuations in fluorescent protein intensity that originate from different pixels along a microscope line (or frame) scan data acquisition that are separated by a set distance (δr). **b**, pCF analysis can be performed at different δr across a line scan to obtain insight into the spatiotemporal evolution of molecular transport. **c**, pCF analysis can be performed at a fixed δr across a line scan to map change in the arrival time of molecular trafficking events with respect to intracellular barriers. The different colors in the bottom panels of **a** and **b** correspond to different δr for the pCF calculation, while $G_{(\tau)}$ and $G_{(\tau, \delta r)}$ in **b** and **c** correspond to correlation amplitude. Max., maximum; Min., minimum.

tracked as a function of its interaction with, or release from, a spectrally distinct fluorescent ligand[1]. The protocol presented here is intended to make pair correlation microscopy an accessible tool for spatiotemporally mapping the intracellular journey of fluorescent molecules, as well as dissection of the role that intracellular architecture and molecular interaction play in the regulation of molecular transport throughout a living cell.

Development of the protocol

Pair correlation microscopy is a variant of fluorescence correlation spectroscopy (FCS), which was developed to enable the tracking of long-range intracellular molecular transport. This development is important because FCS in its original form is limited to a single-point experiment that measures the local diffusion coefficient of a population of moving fluorescent molecules in a homogeneous solution[18–22] (Fig. 2a) by using a time-autocorrelated analysis of their fluctuations in fluorescent intensity upon passing through the parked illumination volume of either a one-photon confocal or two-photon laser scanning microscope. Thus, in the context of a spatially heterogeneous cell, a single-point FCS experiment can sample only the impact of a single aspect of intracellular architecture on a molecule's diffusion coefficient, and it is unable to interrogate a molecule's diffusive route before crossing the single-point FCS illumination volume. It was therefore apparent that in live cell applications, FCS would benefit from the introduction of a spatial component into the microscope measurement, as well as the correlation function used for fluorescence fluctuation analysis. This realization first led to the development of scanning FCS, a technique in which the illumination volume is moved rapidly with respect to the intracellular landscape along a circle or line scan pattern[23–27] (Fig. 2b), and a time-autocorrelated analysis of the fluorescence fluctuations recorded in each pixel of the pattern scanned enables a molecule's local diffusion coefficient to be quantified as a function of position within a spatially heterogeneous environment. Then, dual-foci FCS, a technique in which two parked illumination volumes are laterally shifted by a fixed distance (δr)[28,29] (Fig. 2c) and a time cross-correlated analysis of the fluorescence fluctuations recorded from these two spatially distinct volumes enable a molecule's local to long-range diffusion coefficient to be quantified between a single pair of points that can span a spatially heterogeneous environment. Finally, pair correlation microscopy was developed through applying the concept of dual-foci FCS to a scanning FCS measurement[1,2,4,5]. This technique uses a time cross-correlated analysis of adjacent pairs of spatially distinct fluorescence fluctuations separated by either a fixed or varied distance (δr) along a line scan[1,2,4,5] (Fig. 2d) to enable a molecule's long-range diffusive route to be tracked as a function of position with respect to a spatially heterogeneous environment and across multiple spatial scales. As with any FCS variant, pair correlation microscopy can be extended to a two-channel acquisition that, alongside a time cross-correlated analysis of adjacent pairs of spatially and spectrally distinct fluorescence fluctuations[1] (Fig. 2e,f), enables the impact of molecular complex formation on a diffusive route to be dissected. In this protocol, we first detail the procedure for single-channel line scan pair correlation microscopy data acquisition and analysis, and then we describe how this baseline procedure can be adapted into a two-channel cross-pair correlation microscopy pipeline.

Overview of the procedure

The basic idea behind pair correlation microscopy is to statistically follow a population of fluorescent molecules moving throughout a cell across multiple spatial scales and then map their arrival time with respect to intracellular barriers that limit diffusion. In the simplest case, this involves calibration of a microscope's single-point illumination volume dimensions (Steps 1–7) and then acquisition of a single-channel line scan with this illumination volume across sub-cellular compartments of interest (Fig. 3a) (Steps 8–16), at a rate that is faster than the rate at which the fluorescent molecules are expected to diffuse across and in between the scanned illumination volume. In this way, fluctuations in fluorescent intensity due to the movement of the fluorescent molecules are captured in each pixel (Steps 17–20)[30]. These temporal fluorescence fluctuations can then be autocorrelated (Step 21) through the application of the autocorrelation function (ACF) in an analogous manner to scanning FCS[23–27] (Fig. 3b) and spatially cross-correlated (Step 21) through the application of the pCF at different

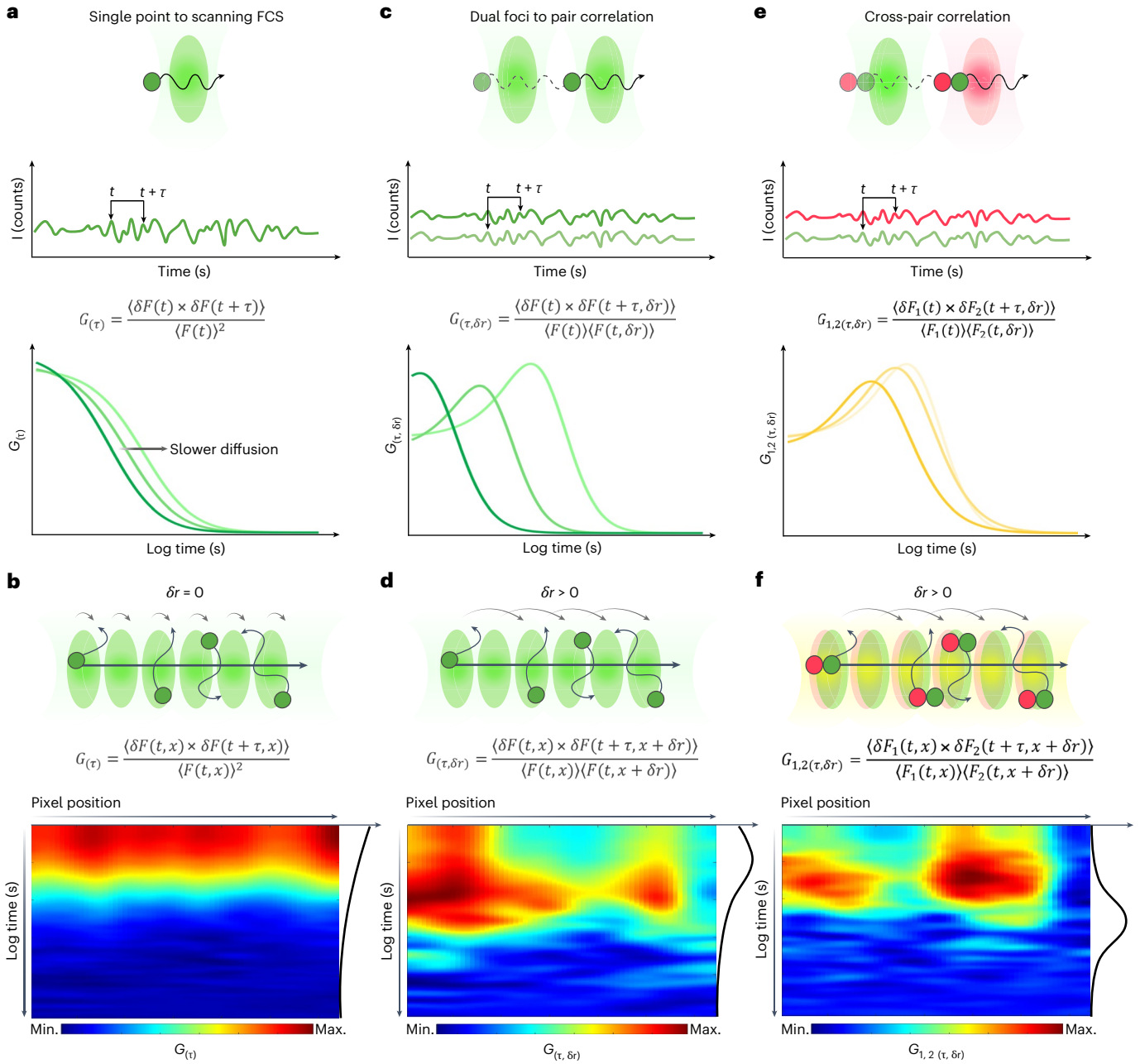

distances ($\delta r > 0$)[2] (Fig. 3c). These analyses collectively produce a series of correlation profile matrices that report molecule number (from the correlation amplitude) and diffusion or arrival time (from the correlation time profile) as a function of pixel position across multiple spatial scales[1]. In each case, the resulting correlation profile matrices are represented as carpets (Fig. 3b,c, bottom panels), which enable direct visualization of subcellular changes in molecular concentration (such as correlation amplitude changes between the cytoplasm and nucleus seen in Fig. 3b) and transport dynamics (such as the delay in arrival time across the nuclear envelope shown in Fig. 3c). These carpet representations can therefore also serve as a guide for how to best extract biological parameters such as concentration, local mobility and diffusive route as a function of space (e.g., column by column versus average across a region of interest (ROI)) and time (e.g., different temporal windows).

Fig. 2 | Evolution from single-point FCS to pCF analysis of a line scan acquisition. a, Single-point FCS involves detection of temporal fluctuations in fluorescence intensity that result from fluorescently labeled molecules diffusing in and out of a small illumination volume, followed by ACF analysis of this signal for every possible delay time (τ) to extract a fluorescent molecule's local diffusion time. $F(t)$ is fluorescence intensity as a function of time t, and $\delta F(t)$ versus $\delta F(t+\tau)$ is the deviation of the fluorescence intensity as a function of time t with respect to the mean $\langle F(t)\rangle$ ($\delta F(t) = F(t) - \langle F(t)\rangle$) versus $\delta F(t)$ shifted by a lag time τ. **b**, Scanning FCS involves rapidly moving the illumination volume with respect to the intracellular landscape and then application of ACF analysis to the temporal fluorescence fluctuations recorded in each pixel position (x) in an analogous manner to single-point FCS, as a means of constructing an ACF carpet (bottom panel) that maps fluorescent molecule local diffusion across a spatially heterogeneous environment. **c**, Dual-foci FCS involves detection of the temporal fluctuations in fluorescence intensity that result from fluorescently labeled molecules diffusing in and out of two small illumination volumes spatially separated by a fixed distance (δr) and then cross-correlation function (CCF) analysis of these two spatially distinct signals for every possible τ to extract a fluorescent molecule's long-range diffusion time. **d**, Pair correlation microscopy involves rapidly moving the illumination volume with respect to the intracellular landscape in an analogous manner to scanning FCS and then application of CCF analysis to pairs of the temporal fluorescence fluctuations recorded in each pixel position (x) separated by a set δr in an analogous manner to dual-foci FCS, as a means of constructing a pCF carpet (bottom panel) that maps fluorescent molecule long-range diffusion across a spatially heterogeneous environment. **e**,**f**, Cross-pair correlation microscopy involves two-channel detection of the temporal fluctuations in fluorescence intensity that result from two spectrally distinct fluorescently labeled molecules diffusing in and out of two small illumination volumes that are rapidly scanned across the intracellular landscape and then CCF analysis of pairs of spatially distinct signals recorded from each channel for every possible τ to enable extraction of a dual-labeled molecule's long-range diffusion time (**e**) and construction of a cross-pCF carpet (bottom panel), which maps this parameter with respect to a spatially heterogeneous environment (**f**). In **b** and **d**, the ACF and pCF carpets were generated by using simulations that considered a homogeneous population ($N = 100$) undergoing isotropic diffusion ($D = 2\ \mu m^2\ s^{-1}$). In **f**, the cross-pCF carpet was generated by using a simulation that considered a heterogenous population ($N_1 = 25$, $N_2 = 37$, $N_{cross} = 37$) undergoing isotropic diffusion ($D_1 = 2\ \mu m^2\ s^{-1}$, $D_2 = 10\ \mu m^2\ s^{-1}$, $D_{cross} = 7\ \mu m^2\ s^{-1}$). In **d** and **f**, the pCF and cross-pCF carpets were calculated at a distance of 400 nm (pCF8). In **a**–**f**, $G_{(\tau)}$, $G_{(\tau,\delta r)}$ and $G_{1,2(\tau,\delta r)}$ correspond to correlation amplitude.

To extract biological parameters of interest from the ACF and pCF correlation carpets, a fit-based approach can be used. Specifically, the columns throughout an ACF carpet can be fit to a diffusion model to recover the average number of molecules (N) from the ACF amplitude (G_0) and their local diffusion coefficient (D_0) (Fig. 3d) (Step 22). By contrast, the columns throughout a pCF carpet can be fit to a probability distribution to recover the following: the time of arrival (τ) for molecules diffusing across δr and the corresponding long-range diffusion coefficient (D_∞) in the instance that δr defines a distance greater than the calibrated confocal beam radial waist (ω_0) (Fig. 3e), the pCF amplitude at the identified τ (G_τ) and the corresponding transport efficiency upon normalization with G_0 from the ACF carpet (G_τ / G_0), and the molecular hindrance imparted by intracellular architecture upon normalization of D_0 from the ACF carpet with D_∞ (D_0/D_∞)[1,5,7] (Fig. 3f) (Step 23). Finally, the bidirectionality (Fig. 3f) and mode of diffusion (Fig. 3g) governing a diffusive route being interrogated across a line scan can also be extracted by reversing the direction of the pCF calculation at any given δr (Fig. 3f) (Step 21), and computation of the molecular mean square displacement (MSD) from multiple pCF carpets can be calculated at different δr[1,4,7] (Fig. 3g) (Step 24). In this protocol, we first detail how to apply this entire analytical workflow to a single-channel CLSM line scan pair correlation microscopy experiment (Steps 17–24). Then, we describe how to extend this pipeline to a two-channel CLSM line scan data acquisition (Fig. 4a) (Steps 25–27), which alongside a spectral cross-ACF and pCF analysis (Fig. 4b,c) (Steps 28–33), enables equivalent biological parameters of interest to be extracted (Fig. 4d–f) as a function of a molecule's association and dissociation with a fluorescent ligand of interest[1,15,31].

Advantages and applications

The key advantage of pair correlation microscopy is its capacity to track long-range intracellular transport with high statistics and single-molecule sensitivity. This advantage arises from the fact that pair correlation microscopy introduces a spatial component into its correlation function, which enables detection of intracellular barriers and their impact on the long-range diffusive route (between non-overlapping illumination volumes) of a population of molecules[30,32–35]. It is for this reason that pair correlation microscopy is particularly advantageous for investigating DNA target search strategies regulated by chromatin network structure[5,7,12–14,16,17,31], nucleocytoplasmic transport regulated by nuclear pore complex architecture[1,4,8–10] and membrane diffusion regulated by the actin cytoskeleton[3,15,36].

Another important advantage of pair correlation microscopy is its amenability to adaptation. For example, the standard implementation of pair correlation microscopy, which is based on a

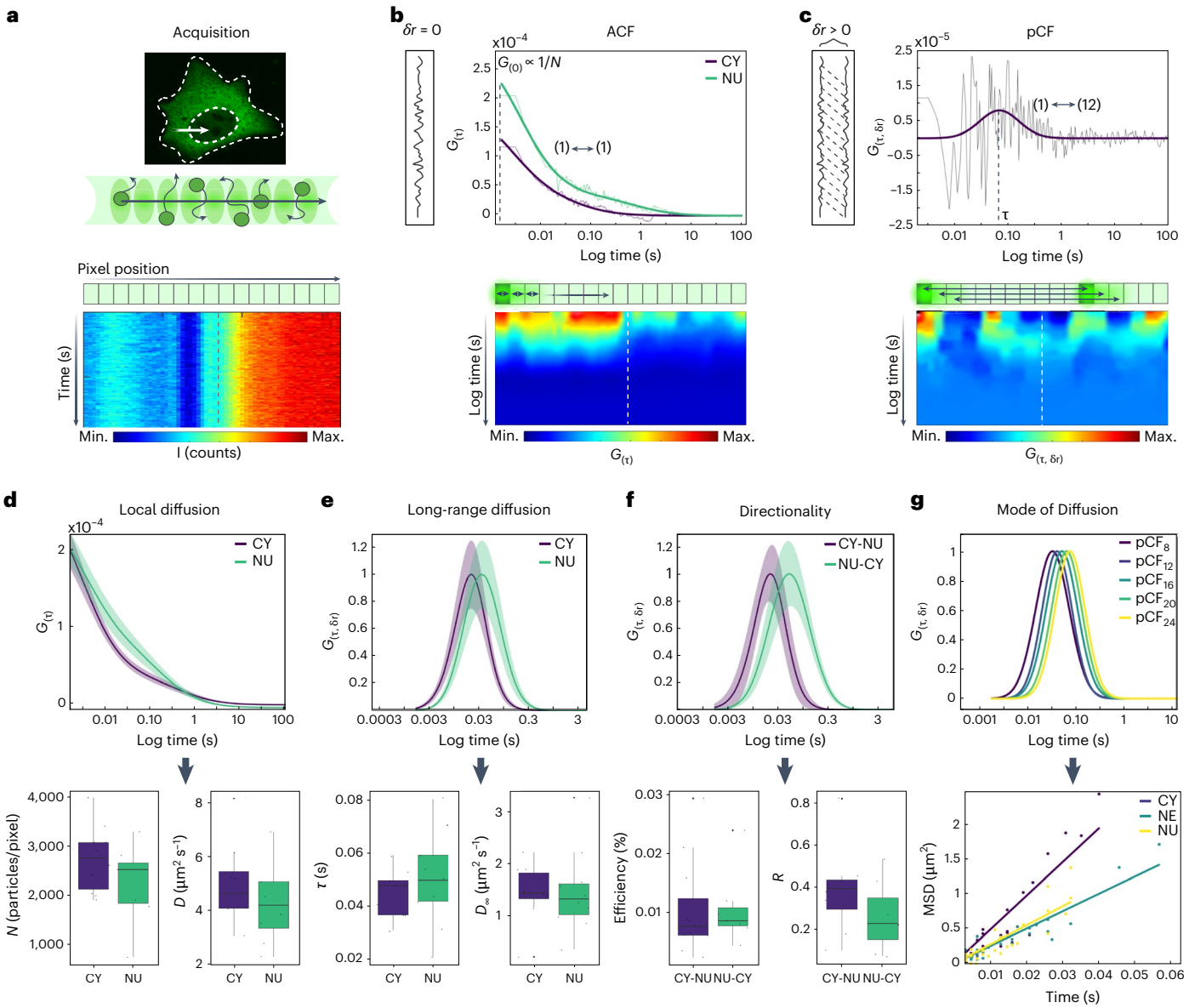

single-channel line scan, can easily be extended to a dual-channel line scan coupled with a cross-pair correlation function to track molecular transport as a function of interaction with a second fluorescent species[1], or to a single-channel frame scan coupled with a radial pCF to track the anisotropy of molecular transport[3,6]. These extensions have enabled the study of the impact of protein-protein interaction on protein trafficking events[31] and the quantification of membrane receptor spatiotemporal dynamics when coupled with total internal reflecting fluorescence (TIRF) microscopy[36]. Pair correlation microscopy has also been multiplexed with different imaging modalities such as stimulated emission depletion microscopy[37] and orbital tracking[8,11] to enable monitoring of diffusion with super-resolution and with respect to a moving structure (e.g., the nuclear pore complex), respectively. Finally, a more recent adaptation of pair correlation microscopy is its application to fluctuations in molecular brightness rather than fluorescence intensity, through the use of a sliding window moment analysis that enables molecular transport to be tracked as a function of oligomeric state[38,39].

In this protocol, we detail how to adapt a single-channel line scan pair correlation microscopy experiment to a dual-channel acquisition that, when coupled with a cross-pCF

Fig. 3 | Overview of the protocol for pair correlation microscopy. **a**, Representative confocal image of a HeLa cell expressing tetrameric enhanced green fluorescent protein (eGFP4), with the line selected for pair correlation microscopy placed across the nuclear envelope (white arrow, top panel). The fluctuations in fluorescence intensity that result from eGFP4 molecules diffusing in and out of pixels along the line scan are recorded and plotted in an intensity carpet representation, where the horizontal *x* axis is pixel position, and the vertical *y* axis is time (bottom panel). **b**, The ACF correlates a fluorescence fluctuation with itself for all possible delay times (τ). This results in an ACF profile with an amplitude (G_0) that is inversely proportional to the number of molecules (N) and a characteristic decay that reports the molecular diffusion coefficient (D) when fitted to a model function. An example ACF profile from a pixel in the cytoplasm (CY) and nucleus (NU) of the line scan in panel **a** are displayed (top panel). The ACF applied to each pixel along the line scan results in an ACF carpet (bottom panel). **c**, The pCF correlates spatially distinct fluorescence fluctuations separated by a set distance ($\delta r = 12$) for all possible τ. This results in a pCF profile with an amplitude indicative of the molecules' transport efficiency and a peak time indicative of the molecules' characteristic arrival time (τ) when fitted to a probability distribution. An example pCF profile from a pair of pixels in the cytoplasm and nucleus of the line scan in panel **a** is displayed (top panel). The pCF applied to each pair of pixels along the line scan results in a pCF carpet (bottom panel). **d**,**e**, A comparison of the model function and probability distribution fits of ACF (**d**) and pCF (**e**) carpets reporting eGFP4 local and long-range diffusion within the cytoplasm and nucleus demonstrates the sensitivity of this technology toward the changes in N, D, τ and long-range diffusion coefficient (D_∞). **f**, The directionality of molecule transport can also be measured by reversing the order of the pCF calculation. For example, pair correlation of fluorescence fluctuations on either side of the nuclear envelope in panel **a** reveals that both the cytoplasm-to-nucleus direction and the nucleus-to-cytoplasm direction enable the detection of molecular diffusion. A comparison of the efficiency of this transit for eGFP4 reveals that molecules with a molecular mass of 108 kDa have reduced cytoplasm-to-nucleus and nucleus-to-cytoplasm transport. The retardation coefficient (R) also shows that the obstruction imposed on eGFP4 in the cytoplasm-to-nucleus direction is greater than in the opposite direction. **g**, The mode of diffusion governing molecule transport can also be measured by calculating the pCF at varied distances (such as $\delta r = 4, 8, 12$) and computation of the MSD from fitted τ values. Each box plot shows the median (middle line) and interquartile range (boxes). The bottom and top of each box indicate the 25th and 75th percentiles, respectively, while whiskers represent the minimum and maximum.

analysis, can track molecule transport as a function of interaction with a ligand. However, the collective suite of adaptations reported here from the literature enable pair correlation microscopy to track and map the direction dependence (anisotropy) of molecular transport as a function of heterotypic and or homotypic interaction.

Limitations

Pair correlation microscopy is restricted by the same issues that limit FCS in general[30]. The key limitations are a reliance on the molecules being tracked exhibiting fluorescence (use of an auto-fluorescent molecule or exogenous label), restricted dynamic range in terms of molecule concentration (<100 nM to prevent loss of amplitude in fluorescence fluctuations), a dependence on rapid line (or frame) scan data acquisition (a sampling frequency that is faster than the timescale of the molecule diffusive dynamics being investigated) and an incompatibility with macromolecular or sample movement (artifacts that introduce unwanted dynamics into the correlation analysis). However, as explained in detail throughout the pair correlation microscopy procedure presented in this protocol, in general, these issues can be addressed through different approaches to sample preparation or cell selection, alongside a spatiotemporally optimized line (or frame) scan and detrending algorithm.

Experimental design

The design of a pair correlation microscopy experiment is underpinned by several important and interconnected considerations that are related to sample preparation, microscope selection and the spatiotemporal dynamics of the molecular transport event being interrogated.

In terms of sample preparation, the most critical requirement for pair correlation microscopy and pCF analysis is that the population of molecules being tracked throughout a living cell must exhibit a bright photostable fluorescence (e.g., that of eGFP) that can be spectrally resolved from other sources of fluorescence present (such as a Hoechst 33342–labeled nucleus), while being present at a sufficiently low concentration (<100 nM) to enable fluctuations in fluorescent intensity that are detectable on a fluorescence microscope and the result of single-molecule dynamics. This requirement also applies to any ligand of interest in the case of cross-pCF analysis; for example, the use of mScarlet alongside eGFP in the presence of Hoechst 33342 would be appropriate in this case.

The most common optical geometry used for pCF and cross-pCF analysis of a single- versus dual-channel 1D line scan experiment is a CLSM, and in this context, the essential hardware requirements are a high numerical aperture objective, such as a 60× water objective with numerical aperture = 1.2, alongside one versus two laser(s) and photon-counting detector(s)

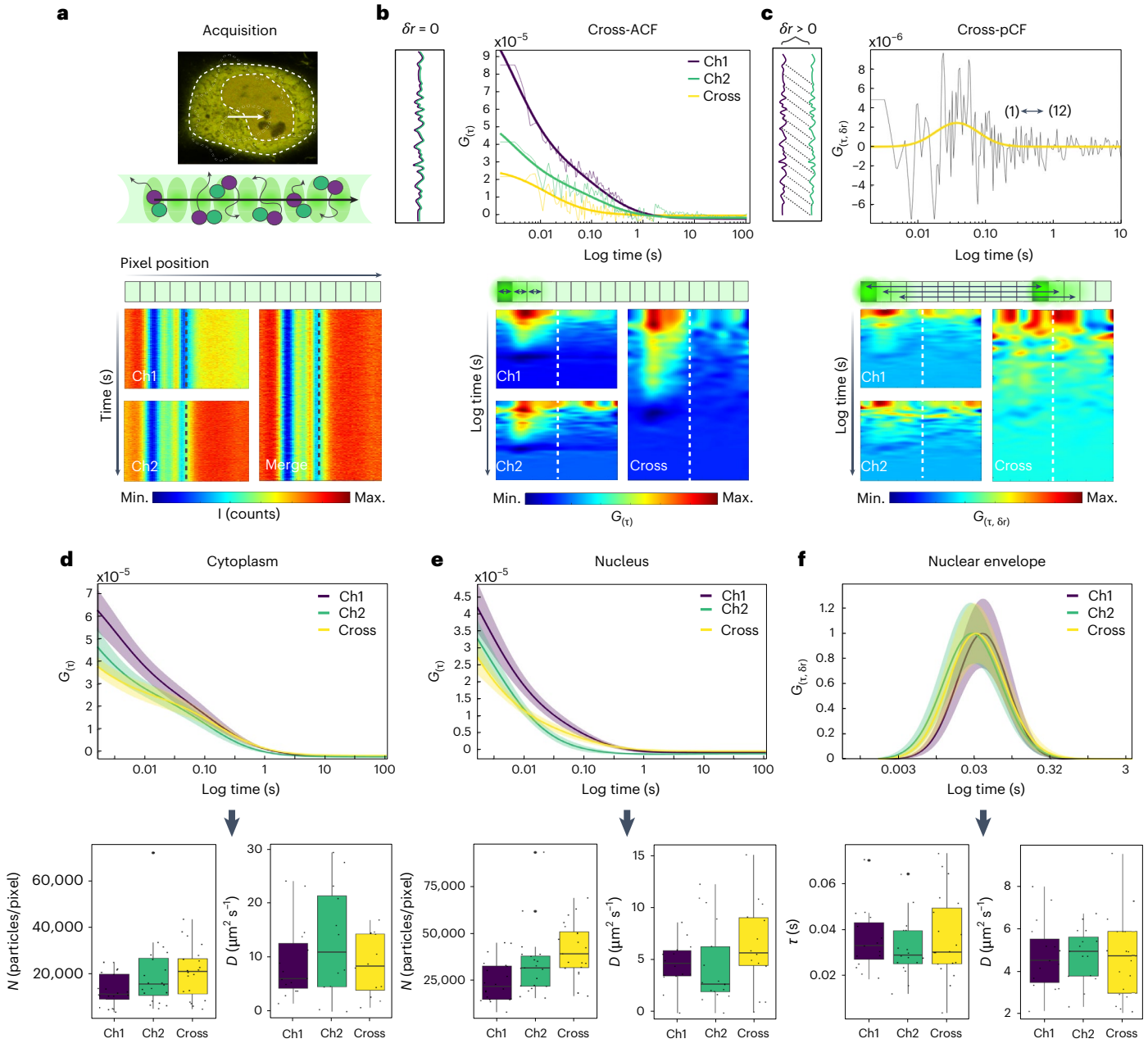

with high efficiency such as a photomultiplier tube (PMT) or single-photon avalanche diode. In principle, however, any optical geometry that gives rise to either a small observation volume being rapidly scanned (e.g., two-photon laser scanning microscopy (LSM)) or multiple effective observation volumes being sampled in parallel (e.g., TIRF or a light sheet geometry) can be used, with the latter scenario being particularly advantageous for radial pCF or cross-pCF analysis of a single- versus dual-channel 2D frame scan experiment.

After sample preparation and microscope selection, the next key consideration for a pair correlation microscopy experiment is the method of data acquisition, and this aspect of the experimental design is largely guided by the spatiotemporal dynamics of the molecular transport event being interrogated. In particular, irrespective of whether the sample demands a single- versus dual-channel acquisition for cross-pCF analysis, or the microscope enables a 1D versus 2D data acquisition for radial pCF analysis, it is critical that the intracellular ROI is

Fig. 4 | Expanding the protocol to cross-pair correlation microscopy of a dual-channel line scan acquisition. a, Representative merged confocal image of a HeLa cell co-transfected with eGFP4 and eGFP fused to mCherry (eGFP-mCherry), with the two-channel line selected for cross-pair correlation microscopy placed across the nuclear envelope (white arrow). The fluctuations in fluorescence intensity that result from eGFP4 and eGFP-mCherry molecules diffusing in and out of pixels along the two-channel line scan are recorded and plotted in intensity carpet representations (bottom panel). Channel 1 (Ch1) contains the fluctuations in intensity due to eGFP4 and eGFP-mCherry molecular mobility, while channel 2 (Ch2) contains the fluctuations in intensity due to eGFP-mCherry mobility. A merged intensity carpet combining the fluctuations in fluorescence intensity from both channels is also shown. **b**, The CCF correlates the fluorescence fluctuations recorded in Ch1 and Ch2 in a single pixel for all possible delay times (τ). This results in a CCF profile with an amplitude (G_{0CC}) that, relative to the limiting amplitude of the ACF profile in Ch1 (G_1) or Ch_2 (G_2), is indicative of the fraction of molecules in a complex (in this case, eGFP-mCherry) and thus a characteristic decay that reports eGFP-mCherry's molecular diffusion coefficient (D) when fitted to a model function. Example CCF and ACF profiles from pixels in the cytoplasm of the line scan in **a** are displayed (top panel). **c**, The cross-pair correlation function (cross-pCF) correlates spatially distinct fluorescence fluctuations recorded in Ch1 and Ch2 that are separated by a set distance ($\delta r = 12$) for all possible τ. This results in a cross-pCF profile with an amplitude indicative of the molecules in a complex transport efficiency (in this case, eGFP-mCherry) and thus a peak time indicative of eGFP-mCherry's characteristic arrival time (τ) when fitted to a probability distribution. An example cross-pCF profile from a pair of pixels in the cytoplasm and nucleus of the line scan in **a** is displayed (top panel). The cross-pCF applied to each pair of pixels along the line scan results in a cross-pCF carpet (bottom panel). **d**, Overlay of ACF analysis of eGFP-mCherry dimer mobility with ACF analysis of total eGFP mobility (Ch1 and Ch2) within the cytoplasm (shading indicates s.e.m.). Solid lines indicate the fitted curve. Boxplots summarizing the average number of molecules (N) and average scale-dependent mobility (D) of eGFP (Ch1 and Ch2) and eGFP-mCherry (cross) are shown ($n = 15$ cells). **e**, Overlay of ACF analysis of eGFP-mCherry dimer mobility with ACF analysis of total eGFP mobility (Ch1 and Ch2) within the nucleus (shading indicates s.e.m.). Boxplots summarizing N and D of eGFP (Ch1 and Ch2) and eGFP-mCherry (cross) are shown ($n = 15$ cells). **f**, Overlay of cross-pCF12 analysis ($\delta r = 960$ nm) of eGFP-mCherry transit with pCF analysis of total eGFP transit (Ch1 and Ch2) across the nuclear envelope (shading indicates s.e.m.). Solid lines indicate the fitted curve. Boxplots summarizing the effective translocation time (τ) and the long-range scale-dependent mobility (D_∞) of eGFP (Ch1 and Ch2) and eGFP-mCherry (cross) are shown ($n = 15$ cells). Each box plot shows the median (middle line) and interquartile range (boxes). The bottom and top of each box indicate the 25th and 75th percentiles, respectively, while whiskers represent the minimum and maximum.

scanned at a rate that is faster than the rate at which the molecules being tracked traverse this environment. Furthermore, the region must be scanned for a length of time that enables the capture of the molecular transport events (specifically, two orders of magnitude longer than the characteristic correlation time).

The final consideration for a pair correlation microscopy experiment is the approach to data analysis, and while this aspect of the experimental design is largely guided by what biological question is being asked, in general, the acquired temporal fluctuations in fluorescence intensity are either spatially cross-correlated at a fixed or varied pCF distance, to enable a molecular transport event to be spatially mapped in terms of arrival time or simply characterized by MSD, respectively.

Materials

Reagents

▲ **CRITICAL** In this section, we list the reagents that have been used for pair correlation microscopy of eGFP in live HeLa cells, alongside calibration of the 488-nm confocal volume with fluorescein. However, note that alternative cell lines, fluorescent proteins and fluorescent dyes can be used. The fluorescent proteins selected should match the laser lines and filters available for a pair correlation microscopy experiment, and the fluorescent dyes used for confocal volume calibration should match the spectral properties of the fluorescent protein/light path being used for a pair correlation microscopy experiment and have a well-characterized diffusion coefficient.

General reagents

- Ultrapure water obtained from a Milli-Q system
- Fluorescein *O*-methacrylate (Sigma, cat. no. 568864)
- Alexa Fluor 568 (Fisher Scientific, cat. no. 11594007)
- NaOH (Sigma, cat. no. S5881)
- High-glucose DMEM (ThermoFisher Scientific, cat. no. 11965092)
- Penicillin-streptomycin (Lonza, cat. no. 17-602E)
- FBS (ThermoFisher Scientific, cat. no. 26140079)

Cell lines and plasmids

- HeLa (American Type Culture Collection, cat. no. CCL-2; RRID: CVCL_0030)
- eGFP and pmCherry plasmids (Addgene, cat. no. 176015; RRID: Addgene_176015; and Addgene, cat. no. 165828; RRID: Addgene_165828, respectively).

Cell culture, plating and transfection

- Glass-bottom culture dishes, 35 mm (0.17 ± 0.1 mm bottom glass thickness) (FluoroDish; WPI, cat. no. FD35-100)
- 1.5H precision glass coverslips (0.17 ± 0.05 mm glass thickness) (Australian Scientific, cat. no. SKU: 0117580)
- Lipofectamine 3000 transfection reagent (ThermoFisher Scientific, cat. no. L3000001)
- Opti-MEM I reduced serum medium (ThermoFisher Scientific, cat. no. 31985062)

Equipment

▲ **CRITICAL** In this section, we list the equipment that has been tested for the application of pair correlation microscopy across a line scan acquisition on an Olympus Fluoview 3000 CLSM. However, note that in principle, any commercial or custom-built CLSM with comparable specifications should also work for line scan pair correlation microscopy experiments. Other microscopy setups such as those based on TIRF[36] or, in theory, a single-plane illumination microscope[40–42] can also be used for a frame scan pair correlation microscopy experiment in conjunction with the 2D pair correlation function[3,6] as discussed under Advantages and applications and Limitations above.

- Olympus Fluoview 3000 inverted CLSM with a galvanometer scanning unit (Olympus IX83 platform with FV31-SU-P scanner; Olympus Corporation, serial no. 7F87906)
- 60× water-immersion objective with a high numerical aperture (1.2) and correction collar for matching the glass thickness used during sample preparation (UPLSAPO60XW; Olympus Corporation, product no. N1480800)
- Solid-state diode laser operating at 488 nm (Olympus Corporation)
- Gallium arsenide phosphide (GaAsP) PMT detectors (FV31-HSD; Olympus Corporation, serial no. 7J40795)
- Stage-top incubator operated at 37 °C with 5% CO_2 (Tokai Hit, serial no. 172239)
- TMC anti-vibration optical table (Newport Corporation, M-VIS3636-SG2-325A)
- Workstation with ≥8 GB of memory, a 64-bit Windows operating system, a solid-state drive with >100 GB and a multi-core processor (HP Z440 base model workstation, serial no. SGH744QL2Z).

Software

- Olympus Fluoview 3000 software for data acquisition
- MATLAB R2022b (or MATLAB runtime for standalone)

Reagent setup

0.01 M NaOH solution

Prepare a 1 M NaOH stock solution by dissolving 0.4 g of NaOH in 10 ml of Milli-Q water (NaOH molecular weight = 40.00 g mol^{-1}). Then, dilute this stock solution to achieve the desired 0.01 M NaOH concentration.

Fluorescein solution

Prepare a 20 nM solution of fluorescein in 0.01 M NaOH. This solution can be stored at 4 °C and will last for several months.

Cell growth medium

Prepare cell growth medium by supplementing high-glucose DMEM with 10% (vol/vol) FBS and 1× penicillin-streptomycin. The medium can be stored at 4 °C for several weeks.

Cell culture, plating and transfection

Culture HeLa cells in a plastic flask partially filled with cell growth medium at 37 °C and in 5% CO_2. 36–48 h before the pair correlation microscopy experiment, when the HeLa cells are 80% confluent, plate 0.3–0.6 million HeLa cells into a 35-mm glass-bottom dish. 12–24 h before the pair correlation microscopy experiment, transfect the plated cells with eGFP (and/or an alternative fluorescent molecule of interest) by using the Lipofectamine 3000 transfection reagent according to the manufacturer's protocol.

Equipment setup

Microscope startup

Turn on the Olympus Fluoview 3000 CLSM components according to the manufacturer's protocol and set the Tokai Hit stage-top incubator to 37 °C with 5% CO_2. Allow the microscope and incubation chamber to equilibrate and stabilize; this can take up to 1 h.

Light path

Open the microscope software, and under 'LSM' mode, set up the light path (laser line, dichroic mirror, band pass filter and detector) that will be used for imaging eGFP (or an alternative fluorescent molecule of interest) by pair correlation microscopy. In the case of eGFP, we use the 488-nm laser coupled with a 488/561/640 dichroic mirror and a GaAsP detector set to collect 500–540 nm light. This light path can also be set up by using the 'Dye' wizard.

Objective

In the microscope software, select the 60× water immersion objective (numerical aperture = 1.2) and check that the objective correction collar is set to a position that falls within the manufacturer's specified glass thickness range for the 35-mm glass-bottom imaging dishes and glass coverslips. For the equipment described here, this is 0.17 mm.

Laser and detector

In the microscope software, set the confocal pinhole to 1 Airy Unit and the power of the 488-nm laser to a low level (e.g., ~1 µW when measured at the objective lens by a power meter), to prevent eGFP photobleaching during pair correlation microscopy experiments. In the microscope software, set the gain of the GaAsP detector to 500 V.

Software installation

Install MATLAB on your computer and download the folder of custom MATLAB code available at https://github.com/ehinde/Pair-correlation-microscopy.

Procedure

Confocal volume calibration and determination of the confocal beam radial waist (ω_0)

● **TIMING 20 min**

▲ **CRITICAL** To calibrate the dimensions of a confocal volume used for a pair correlation microscopy experiment, a single-point fluorescence fluctuation spectroscopy (FFS) experiment must be performed on a fluorescent molecule with a known diffusion coefficient (described below in Steps 1–7). This calibration step enables the radial (ω_0) as well as axial (z_0) waist of the confocal beam to be determined for subsequent ACF analysis of the local diffusion coefficient (D) in each pixel along a line scan (Step 22) and identification of the pCF distance (δr) that will permit long-range transport to be investigated between pixels along a line scan ($\delta r > \omega_0$) (Step 23). In theory, the information from this calibration can also be directly extracted analytically from a pair correlation microscopy line scan fluorescence fluctuation measurement[25].

1. Pipette a drop of ultrapure water onto the 60× water immersion objective lens and then place a #1.5 glass coverslip over the ultrapure water drop on the objective lens and pipette a drop of the 20 nM fluorescein solution onto the glass coverslip.

2. In the microscope software, under the 'Scan Type' window, first select the frame scan option (with a raster scan mechanism) and initiate a 'live scan'. This is a preset frame scan with a low pixel frame size and fast pixel dwell time. During the live scan, check that the GaAsP detector gain is sufficient to observe fluorescence from the fluorescein solution.
3. Under the 'Scan Type' window, select the crosshair for a single point measurement (with no scanning mechanism) and position the crosshair in a central location within the field of view observed during the 'live scan'.
4. Under the 'Scan Setting' window, set the pixel dwell time to a value between 4 and 10 µs to enable a sampling frequency that is 10-fold faster than the time it takes fluorescein molecules to diffuse across the single-point measurement. For example, it takes ~40 µs for fluorescein to diffuse across a radial waist of ~ 0.26 µm with a diffusion coefficient of ~ 440 µm^2, and in this case, a 4-µs dwell time would be suitable.
5. Under 'Time Series', set the scan time to a value between 60 and 200 s to enable a data acquisition that is several orders of magnitude longer than the time it takes fluorescein molecules to diffuse across the single-point measurement and thus permit statistics at longer lag times[43].
6. Select 'LMS start' to initiate the single-point time series experiment. At the end of the data acquisition, save the time series as an .oir file and export as a .csv file.
7. Import the .csv file into MATLAB by opening and running the MATLAB code '*Confocal_Calibration*'. Check that the sampling frequency is set to the inverse of the pixel dwell time used in Step 4. This code will calculate the ACF of the imported single-point FCS experiment recorded in fluorescein and output the single-point confocal volume dimensions (ω_0 and z_0 waist) from a fit of the calculated ACF to a 3D diffusion model. See Box 1 and Supplementary Fig. 1 for more

BOX 1

Calculating the confocal volume from the ACF of a single-point FFS experiment

The '*Confocal_Calibration*' code will first calculate the temporal ACF of the single-point experiment (Eq. 1) that was recorded in 20 nM fluorescein (or another control dye solution) via use of the Wiener–Khinchin theorem (Eq. 2), which says that the correlation function of a signal is equal to the inverse Fourier transform of the signal power spectrum[30].

$$G_{(\tau)} = \frac{\langle \delta F(t) \times \delta F(t+\tau) \rangle}{\langle F(t) \rangle^2} \quad (1)$$

where $F(t)$ is fluorescence intensity as a function of time t, $\delta F(t)$ is the deviation of the fluorescence intensity as a function of time t with respect to the mean $\langle F(t) \rangle$ (also expressed as $F(t) - \langle F(t) \rangle$) and $\delta F(t+\tau)$ is the deviation of the fluorescence intensity as a function of time t with respect to the mean $\langle F(t) \rangle$ shifted by every possible lag time τ.

$$G_{(\tau)} = \frac{\mathcal{F}^{-1}\{\mathcal{F}(F(t))\mathcal{F}^*(F(t+\tau))\}}{\langle F(t) \rangle^2} \quad (2)$$

where $\mathcal{F}$ and $\mathcal{F}^{-1}$ denote the direct and inverse Fourier transform, respectively, and the asterisk signifies complex conjugation.

This calculation will result in a single ACF plotted on a log binned time axis that will then be fit to a one-component diffusion constant model that assumes that the PSF of the one-photon confocal volume is a 3D Gaussian (Eq. 3)[30] through the use of the nonlinear least squares method without weights. Alternatively, to improve the accuracy of parameter estimation, multiple single-point FFS experiments can be acquired and imported into MATLAB for confocal volume calibration, and their average ACF fit via use of the nonlinear least squares method with weights that account for their average ACF's s.e.m.[48].

$$G_{(\tau)} = A\left(1 + \frac{4D\tau}{\omega_0^2}\right)^{-1}\left(1 + \frac{4D\tau}{\omega_0^2 S^2}\right)^{-1/2} + y_0 \quad (3)$$

where A is the correlation amplitude (G_0), D is the diffusion coefficient, τ is the lag time, S is the structure factor that is derived from the ratio of the length (z_0) and the width (ω_0) of the 3D Gaussian observation volume in the focal plane ($S = z_0/\omega_0$) and y_0 is the baseline correction term (offset).

In either case, the ACF fit will output the confocal volume radial (ω_0) and axial (z_0) waist of the confocal volume from the structural parameter (S) by fixing D to a known diffusion coefficient (e.g., fixing D to 440 ± 24 µm^2 s^{-1} for 20 nM of fluorescein at 37 °C in an aqueous solution)[53,56–58]. From ω_0 and z_0, the effective confocal volume (V_{eff}) (where $V_{eff} = \pi^{3/2}{\omega_0}^2 z_0$) can also be calculated for subsequent concentration analysis (Supplementary Fig. 1).

information on how the ACF is calculated and fit to recover ω_0 and z_0. These dimensions will be used in Steps 22 and 23 to process line scans by ACF and pCF analysis, respectively.
▲ **CRITICAL STEP** The '*Confocal_Calibration*' code also imports data in a batch mode to help automate data processing and enable fitting of calculated ACF plots with weights as described in Box 1.
▲ **CRITICAL STEP** The confocal volume is modulated by laser wavelength and power as a result of diffraction[44,45] and fluorescence excitation saturation effects[46,47], respectively. Therefore, calibration of the confocal volume from the confocal beam radial versus axial waist is required every time that a different laser line or power is used for acquisition of pair correlation microscopy data.
◆ **TROUBLESHOOTING**

Pair correlation microscopy data acquisition in a living cell

● **TIMING 10 min per line scan experiment**

▲ **CRITICAL** Pair correlation microscopy of intracellular molecular transport relies on acquisition of a line scan FFS experiment across a population of fluorescent molecules diffusing throughout a living cell. This experiment involves, first, acquiring frame scan images of a selected cell and ROI within the selected cell to collectively guide where to position a high digital zoom line scan with respect to intracellular architecture (Steps 8–12) and then, acquisition of a line scan with sufficient spatiotemporal resolution to enable autocorrelation and pair correlation analysis of the short-to-long-range diffusive route that fluorescent molecules adopt within and between pairs of pixels separated by distances set by the line scan dimensions (Steps 13–16).

8. Pipette a drop of ultrapure water onto the 60× water immersion objective lens and then place a 35-mm glass-bottom culture dish (0.17-mm-thick glass) plated with cells expressing eGFP (or an alternative fluorescent protein) into the microscope stage holder, which floats this sample just above the objective lens.
9. In the microscope software, switch from 'LSM' mode to the 'Ocular' setting and select the epifluorescence light path that enables the fluorescent signal from the cells expressing eGFP to be observed. Adjust the position of the objective until the eGFP-transfected cells are in the objective's focal plane and search for a cell exhibiting a very low level of eGFP expression (<100 nM).
10. Switch back to 'LSM' mode, set 'Scan Type' to frame scan and initiate a 'live scan' (a preset Olympus Fluoview 3000 frame scan with a low pixel frame size and fast pixel dwell time). During the live scan, check that the selected cell is in focus and that the GaAsP detector gain is sufficient to observe fluorescence from the eGFP transfection.
11. Set up an ROI with a digital zoom that contains the entirety of the selected cell (e.g., an ROI of 20–30 μm^2), and then under 'Scan Setting', set the pixel frame size to 512 × 512 and the pixel dwell time to any value between 10 and 20 µs to enable capture of a high-resolution image of eGFP localization with respect to intracellular architecture.
12. Select 'LMS start' and acquire the high-resolution image of eGFP localization throughout the entirety of the selected cell. Within this field of view, set up a new ROI that contains only the intracellular environment of interest for probing eGFP transport via use of a higher digital zoom (e.g., an ROI ≤5 μm^2) and acquire an image within this new ROI by using the lower pixel frame size of 64 × 64, the pixel dwell time used in Step 11 and 'LSM start'.
13. Under the 'Scan Type' window, select the line scan option (with a raster scan mechanism) and position a line scan across the high digital zoom ROI field of view that has an orientation and length that traverses the intracellular route and/or barriers of interest for probing eGFP transport (e.g., a horizontal 5-µm line across an ROI containing a vertical nuclear envelope).
14. Under the 'Scan Setting' window, maintain the pixel line size low at 64. Set the pixel dwell time to any value between 4 and 10 µs that enables a line time, and therefore sampling frequency, that is faster than the time it takes an eGFP-labeled molecule to diffuse across a single confocal observation volume (as defined by ω_0 calibrated in Steps 1–7) or a distance greater than ω_0 as defined by the pixels in the line scan. For example, an 8-µs pixel dwell time across a 64-pixel line size will give a line time of 1.624 ms, which is faster than the 1.69 ms that

it takes for an eGFP-labeled molecule with a 10 μm^2 s^{-1} diffusion coefficient to diffuse across ω_0 ~0.26 μm. See Box 2 and Fig. 5 for how to approximate a molecule's translocation time (τ_D) across the confocal volume versus a longer distance from a reported diffusion coefficient.

15. Under 'Time Series', set the scan time to ≥200 s (≥1 × 10^5 lines per scan) to enable a data acquisition that is several orders of magnitude longer than the time it takes eGFP molecules to diffuse across the line scan and thus permits statistics at longer lag times.
16. Select 'LMS start' to initiate the line scan experiment. At the end of the data acquisition, save the time series as a .oir file and export the line scan data acquisition as a .TIFF file.
    ▲ **CRITICAL STEP** An example of how to translate the pair correlation microscopy data acquisition workflow in Steps 8–16 to an alternative CLSM instrument is provided in Supplementary Note 1.
    ◆ **TROUBLESHOOTING**

Pair correlation microscopy data analysis of molecular transport

● **TIMING 60 min for optimization and 10 min per line scan**

▲ **CRITICAL** Pair correlation analysis of the short-to-long-range diffusive route that fluorescent molecules adopt across a line scan measurement begins with the construction of the acquired fluorescence fluctuations into an intensity carpet (Steps 17–20). The diffusing molecules' local diffusion coefficient (D_0) and effective translocation time (τ) across different spatial scales (δr), which are defined by the line scan's dimensions, are then extracted as a function of pixel position through the application of a fitting procedure to a moving ACF and pCF calculation (Steps 21–23). It is important to note that for spatial scales larger than the confocal volume radial waist ($\delta r > \omega_0$), the geometry of the confocal volume has negligible impact on the shape of the recovered correlation profile[7], and it becomes increasingly difficult to model what happens between two spatially distinct observation volumes in a heterogeneous environment. Thus, while extraction of D_0 benefits from fitting the recovered ACF profiles to a model function (e.g., one-component diffusion constant 3D Gaussian) (Step 22), τ can be simply obtained from the recovered pCF profiles' maximum amplitude and translation of this parameter to an apparent diffusion coefficient (D_∞) (Step 23).

BOX 2

Spatiotemporal considerations for line scan sampling frequency

The sampling frequency of a single-point or line scan FFS measurement limits the range of diffusive dynamics that can be measured across or between a parked or scanned confocal observation volume[30]. This is because a molecule's diffusive dynamics can be detected only if the frequency at which the parked or scanned confocal observation volume is sampled is faster than the time it takes the molecules of interest to translocate (τ_D) across the confocal observation volume's radial waist (ω_0) or some distance of interest (>ω_0) that is defined by the line scan's dimensions. τ_D depends on the molecules' diffusion coefficient (D) (Eq. 4), and if D is known, then the expected τ_D to cross-ω_0 can be calculated and compared with the single-point or line scan sampling frequency that occurs on a micro-to-millisecond timescale, respectively.

$$\tau_D = \frac{\omega_0^2}{4D} \quad (4)$$

For example, if an eGFP-tagged protein of interest is known to exhibit on average an intracellular diffusion coefficient of 10 μm^2 s^{-1}, and the confocal radial waist used to measure this molecule's dynamics is ~0.26 μm, then τ_D would correspond to ~1.69 ms, and a sampling frequency of >592 cycles s^{-1} is required (>1/1.69 ms). For a single-point measurement in which the sampling frequency depends on only the pixel dwell time, detection of fast diffusion coefficients within a confocal observation volume is not a problem (e.g., a 10-μs pixel dwell time results in 100,000 cycles s^{-1}). However, for a line scan measurement in which the sampling frequency depends on the line time (which in turn is contingent on the line pixel dwell time, pixel number and length as a result of the raster scan mechanism) (Fig. 5a,b), detection of fast diffusion coefficients on a local scale (within a single confocal observation volume) can be challenging (e.g., a 1.624-ms line time results in a 616 cycles s^{-1} sampling frequency, which is close to the required 592 cycles s^{-1}). In these cases, however, the fast-diffusing species can usually be caught within a spatially distinct observation volume defined by the line scan upon pair correlation analysis. For example, if an eGFP-tagged protein of interest is freely diffusing at 10 μm^2 s^{-1} between two non-overlapping observation volumes separated by a distance of 0.52 μm, then the predicted τ_D is ~6.75 ms, and a sampling frequency of only >148 cycles s^{-1} is required (the original line time of 1.624 ms with a 616 cycles s^{-1} sampling frequency is now well above this rate).

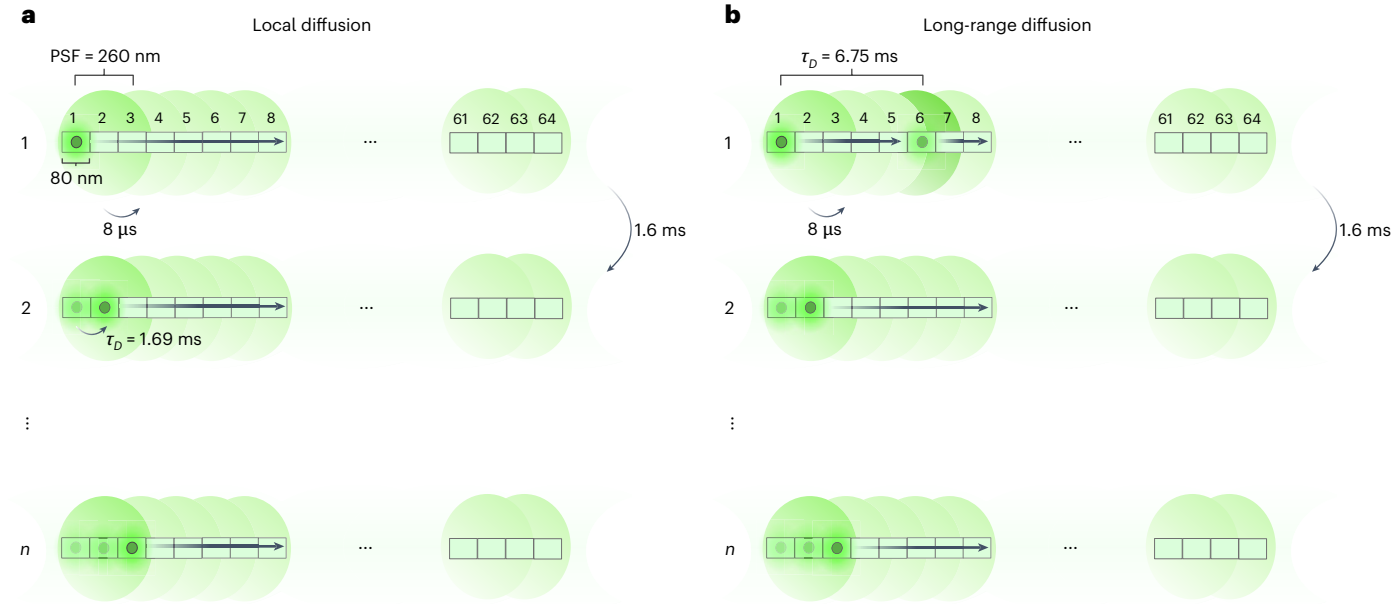

Fig. 5 | Schematic illustration of a line scan acquisition for pair correlation microscopy. a, During a line scan acquisition, fluctuations in fluorescence intensity are acquired by rapidly scanning a laser beam along a line. Two key properties of a line scan that are important for pair correlation microscopy are the line scan's spatial dimensions (pixel size versus line length) and sampling frequency (pixel dwell time versus line time). In general, fluctuations in fluorescence intensity are spatially oversampled with respect to the PSF radial waist (ω_0) at a rate that gives rise to the maximum scanning speed and a short line time. For example, for a PSF of ~260 nm full-width at half-maximum moving along a selected 5.12-µm line scan (64 pixels), the fluctuations in fluorescence intensity are sampled every 80 nm (pixel size), and with an 8-µs pixel dwell time, these scan settings result in a line time of 1.624 ms. The line time includes the time taken for the laser beam to retrace the line scan dimensions. **b**, A molecule's local to long-range diffusive dynamics can only be detected if the line time (1.624 ms) is faster than the time it takes the molecules of interest to translocate (τ_D) across the observation volume PSF (0.26 µm) or some distance of interest greater than the PSF (e.g., between two non-overlapping observation volumes at 0.52 µm. For example, when considering a molecule with an intracellular diffusion coefficient of 10 $\mu m^2 s^{-1}$, τ_D is 1.69 ms for 0.26 µm and 6.75 ms for 0.52 µm. See Box 2 for how to approximate a molecule's τ_D.

17. Import a pair correlation microscopy line scan .TIFF file into MATLAB by opening the MATLAB custom code '*PCF_workflow*' and running the section titled 'Open TIFF file'.
▲ **CRITICAL STEP** The '*PCF_workflow*' code also imports data in a batch mode to help automate data processing once a data-analysis workflow incorporating the following steps has been optimized.
18. Construct the imported line scan into an intensity carpet (*x* axis = pixel position; *y* axis = time) by running the section titled '*Visualize Intensity Carpet*' and inspect the data for slow timescale artifacts such as photobleaching or radial cell movement in the *x*–*y* direction (Supplementary Fig. 2a).
19. If slow timescale artifacts are present in the imported line scan's intensity carpet, then run the section titled '*Detrend Data*' on the most-stable temporal segment of the line scan acquisition. We suggest running on line 2×10^4 onward to avoid initial photobleaching. '*Detrend Data*' will then apply a moving average calculation to each column of the selected intensity carpet segment, by using a set temporal window (i.e., '*binsize*') (e.g., 5,000 lines) that should ideally remove slow timescale trends (e.g., 5,000 × 1.624 ms lines correspond to approximately ≥10 s) without affecting the faster timescale fluorescent molecule dynamics that are of interest (e.g., τ_D of approximately ≤100 ms) (e.g., Supplementary Fig. 2).
20. Construct the detrended line scan into an intensity carpet by again running the section titled '*Visualize Intensity Carpet*' and identify a column range within the detrended intensity carpet that is of interest for ACF and pCF analysis (e.g., columns inside the cytoplasm or nucleus). Then, run the section titled '*Columns to be analysed*' with the first versus last column of the range defined ('*mfirstCol*' and '*mlastCol*').
◆ **TROUBLESHOOTING**

BOX 3

Calculating the ACF and pCF carpets of a line scan FFS experiment

The '*PCF_workflow*' will calculate the temporal ACF of each column within an identified column range of the detrended intensity carpet (Eq. 5) (like scanning FCS) by using the Wiener–Khinchin theorem[30] (Eq. 6) if no spatial distance is set for the temporal cross-correlation (*radius* = 0 pixels) and will output an ACF carpet with an equivalent number of columns to the input (*x* axis = pixel position; *y* axis = log binned time) and a spatial average of the ACF carpet (1 log binned correlation profile).

$$G_{(\tau)} = \frac{\langle \delta F(t,x) \times \delta F(t+\tau,x) \rangle}{\langle F(t,x) \rangle^2} \quad (5)$$

where $F(t,x)$ is fluorescence intensity as a function of time t at pixel position x, $\delta F(t,x)$ is the deviation of the fluorescence intensity as a function of time t with respect to the mean $\langle F(t,x) \rangle$ (also expressed as $F(t,x) - \langle F(t,x) \rangle$) at pixel position x and $\delta F(t+\tau,x)$ is the deviation of the fluorescence intensity as a function of time t with respect to the mean $\langle F(t,x) \rangle$ shifted by every possible lag time τ at pixel position x.

$$G_{(\tau)} = \frac{\mathcal{F}^{-1}\{\mathcal{F}(F(t,x))\mathcal{F}^*(F(t+\tau,x))\}}{\langle F(t,x) \rangle^2} \quad (6)$$

where $\mathcal{F}$ and $\mathcal{F}^{-1}$ denote the direct and inverse Fourier transform, respectively, and the asterisk signifies complex conjugation.

If a spatial distance is set for the temporal cross-correlation (*radius* > 0 pixels), then the '*PCF_workflow*' will calculate the temporal pCF between pairs of columns separated by the set distance within the identified column range of the intensity carpet (Eq. 7) via use of the Wiener–Khinchin theorem (Eq. 8). This will output a pCF carpet with either an equivalent number of columns to the input (*x* axis = pixel position; *y* axis = log binned time) or in the case in which an entire intensity carpet is analyzed, a reduced number of columns to the input (*x* axis = pixel position – set '*radius*', *y* axis = log binned time), and a spatial average of the pCF carpet (1 log binned correlation profile).

$$G_{(\tau,\delta r)} = \frac{\langle \delta F(t,x) \times \delta F(t+\tau,x+\delta r) \rangle}{\langle F(t,x) \rangle \langle F(t,x+\delta r) \rangle} \quad (7)$$

where $F(t,x)$ is fluorescence intensity as a function of time t at pixel position x, $F(t,x+\delta r)$ is fluorescence intensity as a function of time t at a pixel position spatially shifted by δr with respect to pixel position x, $\delta F(t,x)$ is the deviation of the fluorescence intensity as a function of time t with respect to the mean $\langle F(t,x) \rangle$ (also expressed as $F(t,x) - \langle F(t,x) \rangle$) at pixel position x and $\delta F(t+\tau,x+\delta r)$ is the deviation of the fluorescence intensity as a function of time t with respect to the mean $\langle F(t,x+\delta r) \rangle$ shifted by every possible lag time τ at pixel position $x+\delta r$.

$$G_{(\tau,\delta r)} = \frac{\mathcal{F}^{-1}\{\mathcal{F}(F(t,x))\mathcal{F}^*(F(t+\tau,x+\delta r))\}}{\langle F(t,x) \rangle \langle F(t,x+\delta r) \rangle} \quad (8)$$

where$\mathcal{F}$ and $\mathcal{F}^{-1}$ denote the direct and inverse Fourier transform, respectively, and the asterisk signifies complex conjugation.

21. Perform ACF or pCF analysis within or between columns that originate from the column range identified in the detrended intensity carpet in Step 20 by running the section titled '*Get input parameters and calculate ACF or pCF*'; set the sampling frequency ('*sampleFreq*') to the inverse of the line time and the spatial distance for temporal cross-correlation of columns ('*radius*') to 0 pixels if calculating ACF, or a value >0 pixels if calculating pCF. This part of the code will then output an ACF or pCF carpet (where the *x* axis = pixel position, and *y* axis = log binned time) and its associated spatial average (1 log binned correlation profile). See Box 3 for more information on how the ACF and pCF carpets are calculated and spatially averaged.
▲ **CRITICAL STEP** In general, both ACF and pCF analyses are performed so that both short- and long-range diffusion can be analyzed across a line scan. In addition, there is an option to reverse the order of input for the pCF calculation when using the '*Get input parameters and calculate ACF or pCF*' section of the code in Step 21. This option is not relevant for ACF analysis, but for pCF analysis, it enables the directionality of transport between pairs of points along the detrended intensity carpet to be studied, and this capability can be used for pCF analysis by setting '*ReverseOrder* = true'.
▲ **CRITICAL STEP** The spatial distance set for pCF analysis in Step 21 (the radius that is equivalent to δr) is defined in terms of pixels and should be selected to probe molecular transport across a spatial scale that is relevant to the biological question of interest. For example, for a 5-µm, 64-pixel line with a pixel size of ~80 nm, $\delta r = 8$ corresponds to 640 nm. An important consideration when selecting this distance in pixel number is how it compares to the radial waist (ω_0) of the calibrated confocal volume. To probe transport between two observation volumes, and not local diffusion within a single observation volume, this distance should be greater than ω_0; for example, for a 5-µm, 64-pixel line with a pixel size of

~80 nm that is scanned with an ~260-nm radial waist beam, $\delta r < 4$ will probe local diffusion whereas $\delta r > 4$ will probe transport between volumes.

◆ **TROUBLESHOOTING**

22. If in Step 21 *radius* = 0 pixels, then fit the ACF carpet (*x* log binned correlation profiles) or a spatial average of the ACF carpet (1 log binned correlation profile) to a one-component diffusion constant model (Eq. 3 in Box 1) or an alternative model from Table 1 (such as two-component or anomalous diffusion) by running the section titled '*Fit ACF to a model function*'.
▲ **CRITICAL STEP** The fitting method uses the nonlinear least squares method either without or with weights that account for the ACF's s.e.m., respectively. In the latter case, the s.e.m. is calculated point by point from the *x* log binned correlation profiles that underpin the spatial average of the ACF carpet, and incorporation of this information into the nonlinear least squares fit improves the accuracy of parameter estimation[48]. In either case, each ACF fit will output for every correlation profile analyzed the molecule number (N) from the inverse of the correlation amplitude (A) (G_0) multiplied by a shape factor (γ) for a 3D Gaussian point spread function (PSF) ($\gamma_{3D\,Gaussian} = 0.354$) and their local diffusion coefficient (D) when the confocal volume dimensions (ω_0 and z_0) are fixed to the values calibrated in Steps 1–7, and the outputs (A and D) are initialized to appropriate values via the Nelder-Mead Simplex algorithm implemented in the MATLAB function '*fminsearch*'. Typical initialization choices for D are summarized in Table 2.

◆ **TROUBLESHOOTING**

23. If in Step 21 *radius* > 0 pixels, then the pCF carpet (*x* log binned correlation profiles) or a spatial average of the pCF carpet (1 log binned correlation profile) can be fit to either a single Gaussian probability distribution ('*gauss1*') or, in some specific cases, multiple ('*gauss 2*') by running the section titled '*Fit pCF to a Gaussian or model function*'.
▲ **CRITICAL STEP** The fitting method uses the nonlinear least squares method. This fit will output the following for every correlation profile analyzed: the molecules' effective translocation time (τ) across the set spatial scale (δr) from the Gaussian peak position,

Table 1 | Fitting models for the ACF and pCF

Fitting model	Model equation	Refs.
ACF		
One component	$G_{(\tau)} = A\left(1+\frac{4D\tau}{\omega_0^2}\right)^{-1}\left(1+\frac{4D\tau}{\omega_0^2 S^2}\right)^{-1/2} + y_0$	30
Two components	$G_{(\tau)} = A_1\left(1+\frac{4D_1\tau}{\omega_0^2}\right)^{-1}\left(1+\frac{4D_1\tau}{\omega_0^2 S^2}\right)^{-1/2} + A_2\left(1+\frac{4D_2\tau}{\omega_0^2}\right)^{-1}\left(1+\frac{4D_2\tau}{\omega_0^2 S^2}\right)^{-1/2} + y_0$	30,51
Multiple components	$G_{(\tau)} = \frac{\sum_{i=1}^{n} k_i^2 f_i g_{(\tau)}}{N\left(\sum_{i=1}^{n} k_i f_i\right)^2} + y_0$	30
Anomalous diffusion	$G_{(\tau)} = A\left[1+\left(\frac{4D\tau}{\omega_0^2}\right)^{\alpha}\right]^{-1}\left[1+\frac{1}{S^2}\left(\frac{4D\tau}{\omega_0^2}\right)^{\alpha}\right]^{-1/2} + y_0$	52
pCF		
One component	$G_{(\tau)} = A\left(1+\frac{4D\tau}{\omega_0^2}\right)^{-1}\left(1+\frac{4D\tau}{\omega_0^2 S^2}\right)^{-1/2}\exp\left(-\frac{d^2}{\omega_0^2+4D\tau}\right) + y_0$	24,30
Two components	$G_{(\tau)} = A_1\left(1+\frac{4D_1\tau}{\omega_0^2}\right)^{-1}\left(1+\frac{4D_1\tau}{\omega_0^2 S^2}\right)^{-1/2}\exp\left(-\frac{d^2}{\omega_0^2+4D_1\tau}\right) + A_2\left(1+\frac{4D_2\tau}{\omega_0^2}\right)^{-1}\left(1+\frac{4D_2\tau}{\omega_0^2 S^2}\right)^{-1/2}\exp\left(-\frac{d^2}{\omega_0^2+4D_2\tau}\right) + y_0$	30,51
Anomalous diffusion	$G_{(\tau)} = \left[1+\left(\frac{4D\tau}{\omega_0^2}\right)^{\alpha}\right]^{-1}\left[1+\frac{1}{S^2}\left(\frac{4D\tau}{\omega_0^2}\right)^{\alpha}\right]^{-1/2}\exp\left(-\frac{d^2}{\omega_0^2+4D\tau}\right) + y_0$	30

A, correlation amplitude; d, distance between pixels; D, diffusion coefficient; $g_{(\tau)}$, any model described; S, structure factor describing the ellipticity of the detection area, the ratio between the length (z_0) and the width (ω_0) of the 3D Gaussian observation volume in the focal plane ($S = z_0/\omega_0$); y_0, baseline correction term (offset); α, anomalous factor; τ: lag time.

Table 2 | Fit parameter ranges for the diffusion coefficient in FCS measurements

Sample	Diffusion coefficient ($\mu m^2 s^{-1}$)
Dyes in solution	0.01–400 (ref. 42)
Rhodamine 6G, rhodamine green	414 (refs. 49,53–55)
Fluorescein	440 ± 24 (refs. 53,56–58)
eGFP in solution	87 (refs. 59,60)
Proteins in cytoplasm	
eGFP	24–69 (refs. 7,59)
eGFP3	30 (ref. 7)
eGFP5	14 (ref. 7)
STAT2	24 (ref. 7)
Chromodomain	51 (ref. 7)
Proteins in nucleus	
eGFP	30–66 (refs. 5,7,61)
eGFP3	25 (ref. 7)
eGFP5	13 (ref. 7)
Chromodomain	51 (ref. 7)

which in turn can be translated into an apparent diffusion coefficient (D_∞) where $D_\infty = \frac{\langle d \rangle^2}{6\langle \tau \rangle}$ and d is δr in terms of micrometers, or a molecular hindrance coefficient upon normalization with D_0 from the ACF analysis in Steps 21 and 22 (D_∞/D_0)[7]; and the molecules' transport efficiency coefficient from the Gaussian peak amplitude (G_τ) upon normalization with G_0 from the ACF analysis in Step 21 (G_τ/G_0)[5].

▲ **CRITICAL STEP** Although the default setting for extraction of the effective translocation time (τ) and D_∞ from the pCF profiles calculated across different spatial scales (δr) in Step 23 is based on identifying where the maximum correlation amplitude (G_τ) position from a fit to a Gaussian probability distribution is, there is an option in this section of the code to extract this information from a fit with a model function from Table 1 that is equivalent to the model functions used for ACF analysis, but with the diffusion propagator altered to take into account δr[30]. The microsecond time delay between pixels that is introduced by the line scan mechanism is neglected in these model functions, because in the intracellular context, this parameter is significantly smaller than τ_D[24]. In general, we find pCF model fits to work only for processes that are spatiotemporally homogeneous.

◆ **TROUBLESHOOTING**

24. Identify the mode of diffusion governing molecular movement across the detrended intensity carpet (Steps 17–20) by importing this cell array into the MATLAB custom code titled '*Calculate_fit_MSD*', which performs an MSD analysis on the effective translocation times (τ) that result from pCF analysis of the imported cell array across multiple spatial scales (δr). Then, run the subsection 'Fit MSD' to compare the resulting MSD versus τ curves to free diffusion, confined diffusion and/or transient confined diffusion models. See Box 4 for more information on how the MSD plots are calculated and analyzed.

◆ **TROUBLESHOOTING**

Cross-pair correlation analysis of two-channel line scan fluorescence fluctuation experiments

● **TIMING 15 min per line scan experiment (including cell selection), 60 min for optimization of data analysis parameters and then 10 min per line scan experiment in a batch**

▲ **CRITICAL** Pair correlation microscopy of intracellular molecular transport as a function of interaction relies on acquisition of a two-channel line scan FFS experiment across a population of spectrally distinct fluorescent molecules diffusing throughout a living cell (Steps 25–28), and then temporal cross-correlation of the spatially and spectrally distinct fluorescence fluctuations (Steps 29–32). This technique is an adaptation of single-channel pair correlation microscopy.

BOX 4

Calculating MSD from ACF and pCF carpets of a line scan FFS experiment

The '*Calculate_fit_MSD*' code will first calculate the temporal ACF and pCF within versus between pairs of columns separated by an increasing distance (δr = 0, 4, 8, 12, 16, 20, 24, 28 and 32 pixels) across the imported cell array (Eq. 7) via use of the Wiener–Khinchin theorem (Eq. 8) and output the spatial average of each calculated correlation carpet (1 log binned correlation profile for every δr). Then, this code will fit the ACF log binned correlation profile to a diffusion model (Table 1) to output D_0, fit the pCF log binned correlation profiles to Gaussian probability distributions to output the effective translocation time (τ) as a function of δr and use these fit outputs to calculate the MSD[50] (Eq. 9) as a function of δr.

$$\mathrm{MSD} = 2nD_0\tau \tag{9}$$

where n is the dimensionality (3 for intracellular environment), D_0 is the local diffusion coefficient and τ is the effective translocation time for each δr tested.

Finally, this code will then compare a plot of the calculated MSD values versus τ with the following three models to obtain a quantitative insight into the mode of particle motion[7,63]: (i) free diffusion, in which the MSD increases linearly with the time interval (Eq. 10); (ii) confined diffusion, in which a protein molecule undergoes Brownian diffusion within a limited area and cannot move out of the area during the observation period (Eq. 11); and (iii) transient confined diffusion, in which free diffusion is impeded by the presence of obstacles to diffusion for a limited period, after which the molecule is able to diffuse freely (Eq. 12)[64,65].

$$\sigma_r^2(\tau) = 4D\tau + \sigma_0^2, \tag{10}$$

$$\sigma_r^2(\tau) = \frac{L_{\mathrm{conf}}^2}{3}\left(1 - e^{-\frac{\tau}{\tau_c}}\right) + \sigma_0^2, \tag{11}$$

$$\sigma_r^2(\tau) = \frac{L_{conf}^2}{3}\left(1 - e^{-\frac{\tau}{\tau_c}}\right) + 4D_{\mathrm{macro}}\tau + \sigma_0^2, \tag{12}$$

where $\sigma_r^2(\tau)$ is the MSD, L is the linear size of the confinement area, τ_c is an index of how fast confinement occurs and σ_0^2 is equal to ω_0^2 (ref. 63).

25. Modify the reagent and equipment setup such that: (i) a green and red fluorescent dye solution is prepared for confocal volume calibration (e.g., Alexa 568 in addition to fluorescein), (ii) a 35-mm glass-bottom culture dish is plated with adherent cells (such as HeLa cells) co-expressing two biological molecules of interest that are labeled with green and red fluorophores (such as eGFP and mCherry) and (iii) the Olympus Fluoview 3000 CSLM is fitted with 488- and 561-nm laser lines alongside two GaAsP PMTs.
26. Modify the microscope startup and software installation procedure such that under 'LSM' mode in the Olympus FV3000 software the light path is set up to simultaneously image eGFP and mCherry through the use of the 488- and 561-nm laser lines coupled with a 488/561/640 dichroic mirror and two GaAsP detectors set to collect 500–540 and 610–650 nm, respectively.
    ▲ **CRITICAL STEP** Minimizing spectral cross-talk via fluorophore selection and light path setup is critical for cross-pair correlation function analysis of two-channel line scan data; only a small percentage (<5%) of the green fluorophore's signal should bleed through into the red channel[42,49].
27. Modify the confocal volume calibration procedure (Steps 1–7) such that both confocal volumes generated by the 488- and 561-nm laser lines are calibrated via two independent single-point FFS measurements of the green and red fluorescent dyes prepared in Step 25 while using the light path set up in Step 26, with only the relevant laser on in each case.
    ▲ **CRITICAL STEP** This calibration procedure will result in a radial and axial waist for the green channel (ω_{01} and z_{01}) as well as an ~1.5-fold larger radial and axial waist for the red channel (ω_{02} and z_{02})[30]. The apparent radial and axial waist of the cross-correlation volume (ω_{0CC} and z_{0CC}) assuming the CLSM detection volumes are aligned should be approximated as the average.
28. Modify the pair correlation microscopy data acquisition procedure (Steps 8–16) such that: (i) a cell exhibiting low co-expression of eGFP and mCherry (<100 nM) is selected via the ocular, (ii) a two-channel simultaneous frame scan reference image is acquired of the

selected cell and an ROI within this cell by using equivalent settings to Steps 11 and 12, (iii) a two-channel simultaneous line scan time series is acquired across the ROI with equivalent settings to Steps 13–16 and (iv) the resulting line scan acquisition is saved as a .oir file as well as exported as two .TIFF files (for the eGFP channel (Ch1) and mCherry channel (Ch2)) for import into MATLAB.

29. Modify the pair correlation microscopy analysis procedure (Steps 17–24) such that: (i) the two .TIFF files from a single two-channel pair correlation microscopy experiment (Ch1 and Ch2) are imported into MATLAB via the '*crossPCF_workflow*' code and (ii) the workflow of analysis detailed for a single-channel line scan is independently applied to Ch1 and Ch2. This will result in the generation of intensity, ACF and/or pCF carpets for both the eGFP and mCherry channels across an identified column range of interest, as well as output parameters that describe the short-to-long-range diffusive dynamics of all the green and or red molecules that are present.
30. Extract the short- and/or long-range diffusive dynamics of only molecules that are green and red (in a complex) by performing a cross-correlation function (CCF) (no spatial component) and/or cross-pCF analysis between Ch1 and Ch2 within or between columns that originate from the column range identified in Step 29 by running the section titled '*Get input parameters and calculate CCF or cross pCF*'. Set the sampling frequency to the same value used for '*sampleFreq*' in Step 21, and set the spatial distance for temporal cross-correlation of columns to either 0 (CCF) or the same value used for '*radius*' in Step 21 that was greater than 0 (cross-pCF).
31. Fit the CCF carpet (*x* log binned correlation profiles) or a spatial average of the CCF carpet (1 log binned correlation profile) to a one-component diffusion constant model (Eq. 3) or an alternative model from Table 1 in an analogous manner to an ACF (Step 22) by running the section titled '*Fit ACF to a model function*'. For every correlation profile analyzed, this fit will output the following: the cross-correlation amplitude (A) (G_{0CC}) that upon normalization with the autocorrelation amplitude of the limiting individual channel (Ch1 G_{01} or Ch2 G_{02}) reports the fraction of green–red complex present (G_{0CC}/G_{01} if $G_{01} < G_{02}$ or G_{0CC}/G_{02} if $G_{02} < G_{01}$), and the local diffusion coefficient of this green–red complex (D_{0CC}).
32. Fit the cross-pCF carpet (*x* log binned correlation profiles) or a spatial average of the cross-pCF carpet (1 log binned correlation profile) to a Gaussian probability distribution in an analogous manner to a single-channel pCF (Step 23) by running the section titled '*Fit pCF to a Gaussian or model function*'. For every correlation profile analyzed, this fit will output the following: the Gaussian peak position that represents the green–red molecules' effective translocation time (τ_{CC}) across the set spatial scale (δr), as well as the corresponding apparent diffusion coefficient ($D_{\infty CC}$) and molecular hindrance coefficient upon normalization with D_{0CC} from the CCF analysis in Step 31 ($D_{\infty CC}/D_{0CC}$)[7]; and the Gaussian peak amplitude ($G_{\tau CC}$) that upon normalization with the pair correlation amplitude of the limiting individual channel (Ch1 $G_{\tau 1}$ or Ch2 $G_{\tau 2}$) can be translated into the fraction of green–red complex transported ($G_{\tau CC}/G_{\tau 1}$ if $G_{\tau 1} < G_{\tau 2}$ or $G_{\tau CC}/G_{\tau 2}$ if $G_{\tau 2} < G_{\tau 1}$).
33. Extract the mode of diffusion governing the movement of green and red molecules in a complex across a two-channel line scan experiment (Box 5) analogously to a single-channel experiment (Step 24) by importing the cell array corresponding to the detrended intensity carpets of Ch1 and Ch2 into '*Calculate_fit_cross_MSD*'. This code will first calculate the temporal CCF and cross-pCF within versus between pairs of columns separated by an increasing distance (δr = 0, 4, 8, 12, 16, 20, 24, 28 and 32 pixels) across the imported cell arrays (Eq. 15) via use of the Wiener–Khinchin theorem (Eq. 16) and output the spatial average of each calculated correlation carpet. This code will fit the CCF log binned correlation profile to a one-component diffusion constant model (Eq. 3) to output D_{0CC} and fit the pCF log binned correlation profiles to Gaussian probability distributions to output the effective translocation time (τ_{CC}) as a function of δr. Finally, this code will then use these fit outputs to calculate the MSD (Eq. 9)[50] as a function of δr, which can then be tested against three different models (Eqs. 10–12).

BOX 5

Calculating the CCF and cross-pCF carpets of a line scan FFS experiment

If no spatial distance is set for the temporal cross-correlation (*radius* = 0 pixels), then this section of the code will calculate the temporal CCF between Ch1 and Ch2 in each column within the identified column range of the two detrended intensity carpets (Eq. 13) via use of the Wiener–Khinchin theorem (Eq. 14). This will output a CCF carpet with an equivalent number of columns to the input (*x* axis = pixel position; *y* axis = log binned time) and a spatial average of the CCF carpet (1 log binned correlation profile).

$$G_{1,2(\tau)} = \frac{\langle \delta F_1(t,x) \times \delta F_2(t+\tau,x)\rangle}{\langle F_1(t,x)\rangle \langle F_2(t,x)\rangle} \quad (13)$$

where $F_1(t,x)$ and $F_2(t,x)$ is fluorescence intensity as a function of time t at pixel position x in Ch1 versus Ch2, $\delta F_1(t,x)$ is the deviation of the fluorescence intensity as a function of time t with respect to the mean $\langle F_1(t,x)\rangle$ (also expressed as $F_1(t,x) - \langle F_1(t,x)\rangle$) at pixel position x in Ch1 and $\delta F_2(t+\tau,x)$ is the deviation of the fluorescence intensity as a function of time t with respect to the mean $\langle F_2(t,x)\rangle$ shifted by every possible lag time τ at pixel position x in Ch2.

$$G_{(\tau)} = \frac{\mathcal{F}^{-1}\{\mathcal{F}(F_1(t,x))\mathcal{F}^*(F_2(t+\tau,x))\}}{\langle F_1(t,x)\rangle \langle F_2(t,x)\rangle} \quad (14)$$

where $\mathcal{F}$ and $\mathcal{F}^{-1}$ denote the direct and inverse Fourier transform, respectively, and the asterisk signifies complex conjugation.

If a spatial distance is set for the temporal cross-correlation (*radius* > 0 pixels), then this section of the code will calculate the temporal cross-pCF between pairs of columns in Ch1 and Ch2 separated by the set distance within the identified column range of the two detrended intensity carpets (Eq. 15) via use of the Wiener–Khinchin theorem (Eq. 16) and output a cross-pCF carpet with either an equivalent number of columns to the input (*x* axis = pixel position; *y* axis = log binned time) or, in the case in which an entire detrended intensity carpet is analyzed, a reduced number of columns to the input (*x* axis = pixel position – set '*radius*'; *y* axis = log binned time) and a spatial average of the cross-pCF carpet (1 log binned correlation profile).

$$G_{1,2(\tau,\delta r)} = \frac{\langle \delta F_1(t,x) \times \delta F_2(t+\tau,x+\delta r)\rangle}{\langle F_1(t,x)\rangle \langle F_2(t,x+\delta r)\rangle} \quad (15)$$

where $F_1(t,x)$ is fluorescence intensity as a function of time t at pixel position x in Ch1, $F_2(t,x+\delta r)$ is fluorescence intensity as a function of time t at a pixel position spatially shifted by δr with respect to pixel position x in Ch2, $\delta F_1(t,x)$ is the deviation of the fluorescence intensity as a function of time t with respect to the mean $\langle F_1(t,x)\rangle$ (also expressed as $F_1(t,x) - \langle F_1(t,x)\rangle$) at pixel position x in Ch1 and $\delta F_2(t+\tau,x+\delta r)$ is the deviation of the fluorescence intensity as a function of time t with respect to the mean $\langle F_2(t,x+\delta r)\rangle$ shifted by every possible lag time τ at pixel position $x+\delta r$ in Ch2.

$$G_{1,2(\tau,\delta r)} = \frac{\mathcal{F}^{-1}\{\mathcal{F}(F_1(t,x))\mathcal{F}^*(F_2(t+\tau,x+\delta r))\}}{\langle F_1(t,x)\rangle \langle F_2(t,x+\delta r)\rangle} \quad (16)$$

where $\mathcal{F}^{-1}$ and $\mathcal{F}^{-1}$ denote the direct and inverse Fourier transform, respectively, and the asterisk signifies complex conjugation.

Troubleshooting

Troubleshooting advice can be found in Table 3.

Table 3 | Troubleshooting table

Step	Problem	Possible reason	Solution
7	Poor quality single-point FFS data and ACF for confocal volume calibration	High-concentration sample	Reduce concentration of fluorescent calibration solution to ensure that the fluorescence fluctuations detected are due to single fluorescent molecules and to prevent molecule aggregation
		Short measurement time	Increase the total measurement time to permit statistics at long lag times and decrease error of obtained PSF[43]
		Low sampling frequency	Increase the sampling frequency (reduce pixel dwell time) to maximize measurement of fluorescent molecule dynamics
16	Cell movement	Fresh sample on stage	Wait 5–10 minutes for cells to settle in imaging dish and acclimatize to measurement conditions
		Too high laser intensity	Reduce laser intensity to prevent adverse cell reaction to strong laser illumination

Table 3 (continued) | Troubleshooting table

Step	Problem	Possible reason	Solution
20	Poor quality line scan FFS data and intensity carpets	Photobleaching	Reduce laser intensity to prevent major photobleaching. For minor photobleaching, apply a detrending algorithm to selectively remove this slow timescale artifact. In this Protocol, we use a simple moving average for this purpose, e.g., in Supplementary Fig. 3. It is also important to note that several effective alternative detrending algorithms have been reported[62]
		Macromolecular cell movement	Avoid intracellular regions of interest where macromolecular movement is observed (e.g., where vesicles are trafficked). For minor movement, similar to photobleaching, apply a detrending algorithm to selectively remove this slow timescale artifact
21–23	Poor quality ACF and pCF carpets alongside failed fitting	Short measurement time and/or low sampling frequency	Increase the total measurement time and sampling frequency (reduce line time) to permit statistics at long lag times and enable measurement of intracellular fluorescent molecule dynamics (as explained for ACF analysis of single-point FFS data)
		Inadequate model specification and/or starting values for ACF fitting	Use a different diffusion model to fit the ACF that incorporates more parameters, e.g., a model that includes an additional diffusion component or a flow component. Use starting values for the model fit that are biophysically feasible[30]
		Inadequate distance for pCF calculation and/or starting values for Gaussian fitting	Use a different distance (δr) for the pCF calculation to see if the molecule dynamics are better detected on a different spatial scale. Use starting values for the Gaussian fit that are biophysically feasible
24	Poor MSD fitting	Outliers	Plot raw data to identify a threshold that removes outliers prior to MSD fitting
		Inadequate starting values for MSD fitting	Evaluate the initialization values carefully, especially if the size of a confined zone (L within the code) is being considered[63]

Timing

Microscope set up: ~ 60 min
Steps 1–7, calibration measurement and analysis: ~20 min
Steps 8–16, live cell experiment: ~10 min per line scan experiment (including cell selection)
Steps 17–24, line scan experiment analysis (ACF, pCF or MSD): ~60 min for optimization of data-analysis parameters for one type of experiment and then ~10 min per line scan experiment in a batch
Steps 25–33, dual-channel line scan experiment and analysis: ~15 min per line scan experiment (including cell selection), ~ 60 min for optimization of data-analysis parameters and then ~10 min per line scan experiment in a batch

Fig. 6 | Evaluating nanoparticles' subcellular distribution and potential as chemotherapeutic carriers by using the pCF. a, Representative confocal image of an MCF7 cell incubated with fluorescein-labeled nanoparticles. Scale bar, 5 µm. The dotted white line across the extracellular space (EX), cytoplasm (CYTO) and nucleus (NUC) represents the directionality of the line scan. **b**, Intensity carpet of fluorescein-labeled nanoparticles along the scanned line. The x axis represents the pixel's position (64 pixels), and the y axis represents the time. **c**, Intensity profile averaged over time of fluorescein-labeled nanoparticles with respect to pixel position. **d**, Averaged fluorescence intensity of mobile nanoparticles in the extracellular space, cytoplasm and nucleus. **e**–**h**, ACF analysis of intensity fluctuations to quantify mobile fluorescein-labeled nanoparticles with respect to pixel position and subcellular compartment. **e**, ACF is calculated for each pixel and delay time (τ). **f**, ACF carpet. Autocorrelation profile derived for each pixel along the line scan. **g**, Number of mobile fluorescein-labeled nanoparticles (NP) in each pixel, derived from maximum amplitude values. **h**, Average number of nanoparticles in the extracellular space, cytoplasm and nucleus. N values were obtained by ACF analysis. **i**–**l**, Pair correlation analysis of the intensity fluctuations to quantify the translocation of mobile nanoparticles. **i**, pCF at a fixed distance was calculated for each pixel. From its peak, the characteristic transit time describing the mobility within compartments and across barriers is extracted. **j**, pCF carpet. pCF7 profile derived for each pixel in the line scan with δr = 560 nm. **k**, Transit times with respect to pixel position. **l**, Box plot summarizing the transit times of fluorescein-labeled nanoparticles obtained by pCF analysis within the extracellular space, cytoplasm and nucleus and across the extracellular space-to-cytoplasm direction and cytoplasm-to-nucleus direction. **m**,**n**, Box plots summarizing the transit times of fluorescein-labeled micelle- (purple), vesicle- (red), rod- (blue) and worm-(red) shaped nanoparticles within a compartment (extracellular space, cytoplasm and nucleus) (**m**) versus between compartments (across plasma membrane, extracellular space-to-cytoplasm; and across nuclear envelope, cytoplasm-to-nucleus) (**n**) (n = 16 measurements). **o**, Bar graph summarizing the number of doxorubicin (DOX) molecules delivered by Cy5-modified high-aspect-ratio shaped nanoparticles (in this case, worm-shaped nanoparticles) to the cell nucleus when functionalized with or without a nuclear localization signal (NLS) (n = 8 measurements). In **b**, **c**, **f**, **g**, **j** and **k**, the position of the plasma membrane and nuclear envelope are indicated by dotted red and blue lines, respectively. In **d**, **h** and **o**, the mean ± s.d. is indicated in the bar plots. In **l**–**n**, the box plots show the median (middle line) and interquartile range (boxes). The bottom and top of each box indicate the 25th and 75th percentiles, respectively, while whiskers represent the minimum and maximum. *, $P \leq 0.05$, and **, $P \leq 0.01$. ns, non-significant. Figure adapted with permission from ref. 1, Springer Nature.

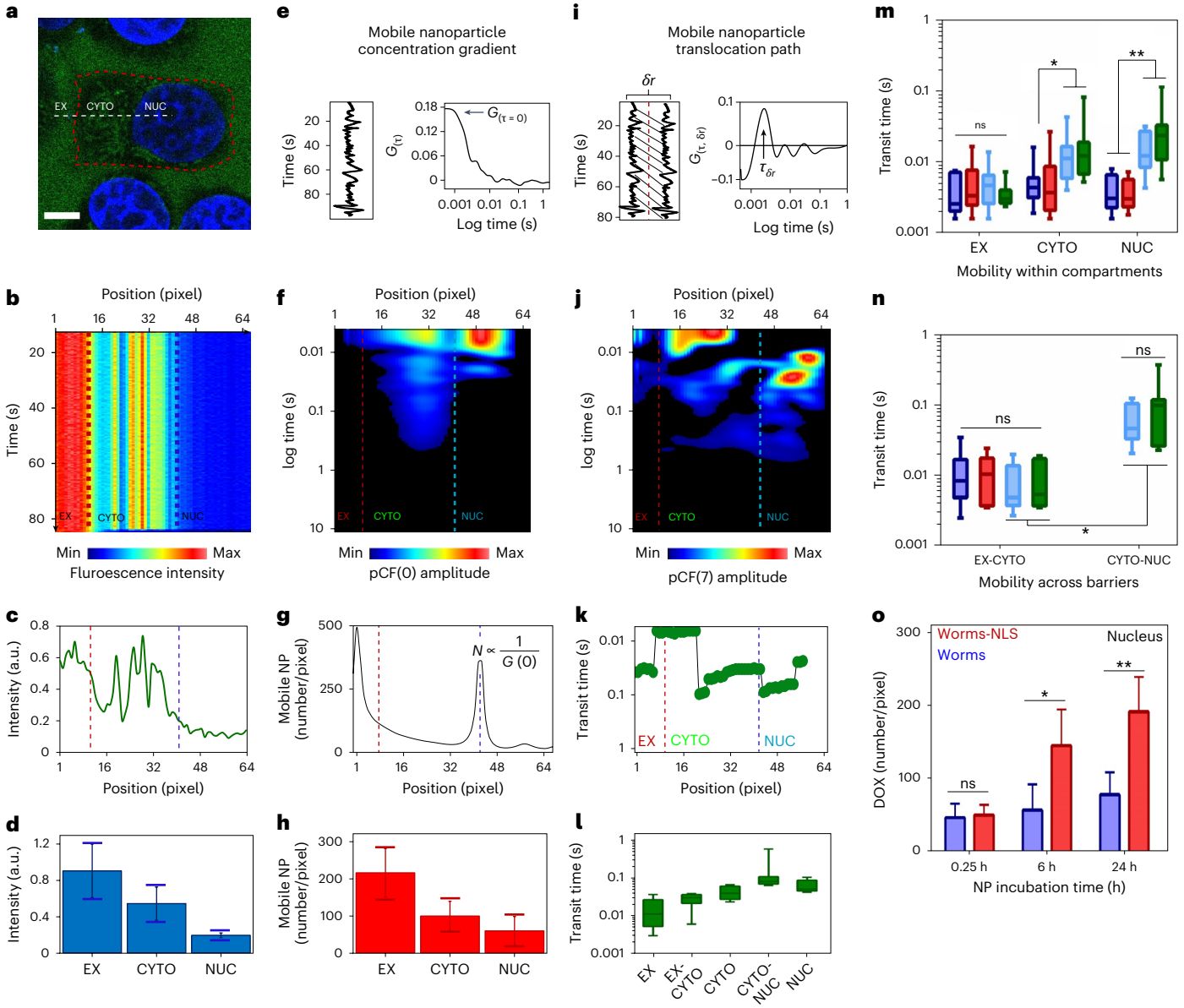

Anticipated results

The protocol described here for pair correlation microscopy provides a means for researchers to spatiotemporally map and quantify the transport mechanism of proteins throughout a single cell. In particular, from acquisition of single- and/or dual-channel line scan FFS experiments across intracellular ROIs, this protocol can be used to first construct ACF, pCF and cross-pCF carpets, which enable exploration of the short-to-long range diffusive route that molecules adopt as a function of direction and or interaction. These ACF, pCF and cross-pCF carpets can then be analyzed and fit to model functions that output biologically relevant parameters, such as molecule number, diffusion coefficient, arrival time or transport efficiency, as a means of enabling a statistical comparison of different protein transport patterns and the accessibility of different intracellular barriers. Along this line, in this section, we present and describe representative pair and cross-pair correlation microscopy results

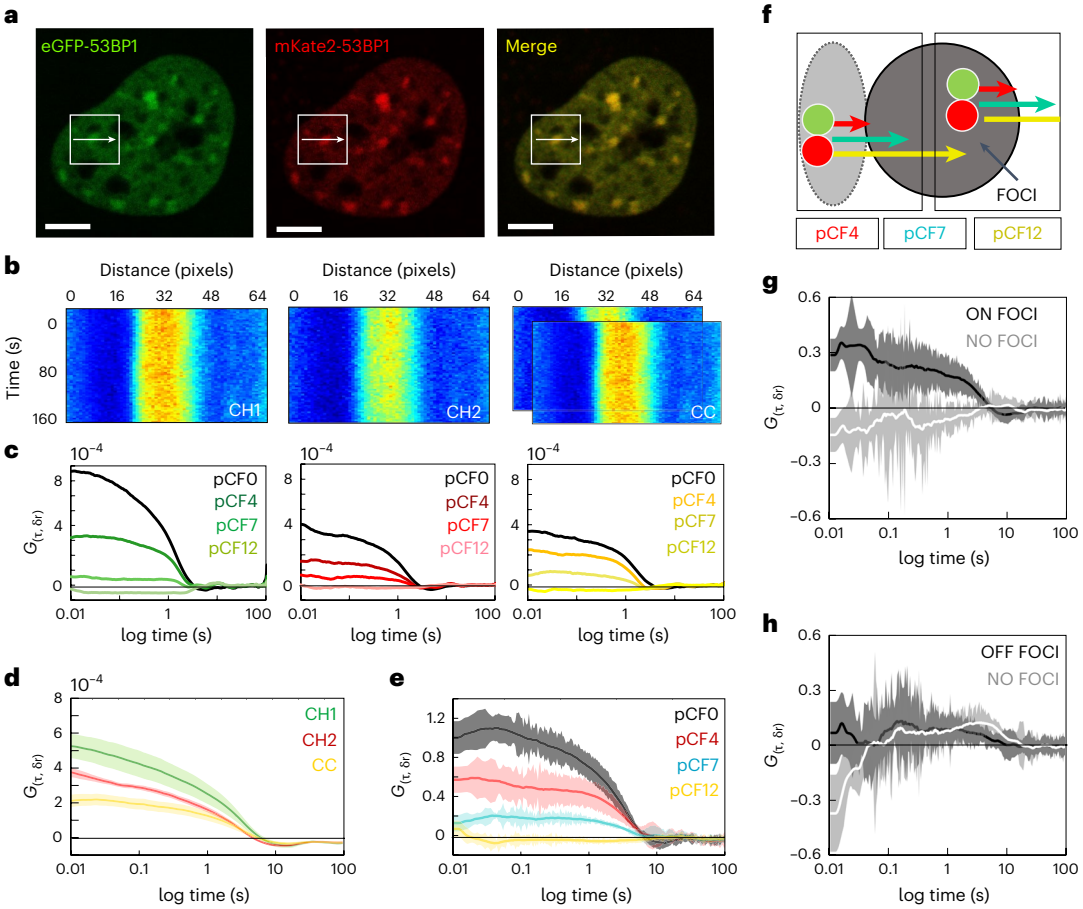

Fig. 7 | Cross-pCF analysis for monitoring 53BP1 dimer recruitment and retention at DNA DSBs. a, Representative confocal image of a DIvA cell nucleus co-transfected with eGFP-53BP1 and mKate-53BP1 after DSB induction. Scale bars, 5 µm. The white arrows across a 53BP1 nuclear condensate formed at a DSB site represent the directionality of the line scan. **b**, Intensity carpets that result from acquisition of a two-channel line scan across the 53BP1 nuclear condensate selected in **a** in the green (Ch1), red (Ch2) and cross-correlated channels (CC). **c**, Optimization of the cross-ACF and pCF analysis between channel Ch1 and Ch2 to track 53BP1 dimer short-to-long-range transport (at $\delta r = 0$, 4, 7 and 12 pixels) as well as comparison with ACF and pCF analysis in the individual channels (Ch1 and Ch2). **d**, Overlay of cross-ACF (pCF0) analysis of 53BP1 dimer mobility (yellow) with pCF0 analysis of total 53BP1 mobility (green and red) to extract the fraction of 53BP1 dimer present in the nucleoplasm ($n = 5$ cells). **e**, Overlay of cross-pCF (pCF4, pCF7 and pCF12) analysis of 53BP1 dimer transport from the nucleoplasm onto a DSB foci normalized with respect to pCF0 to compare transport efficiency ($n = 5$ cells). **f**, Schematic of the spatial evolution of 53BP1 dimer transport onto versus off DSB foci (pCF7 reaches outside the PSF). **g**,**h**, Cross-pCF7 analysis of 53BP1 dimer translocation, both onto (**g**) and off of (**h**) DSB foci, normalized with respect to cross-pCF0 ($n = 5$ cells). Figure adapted with permission from ref. 31, Springer Nature.

that have been published and underpin the development of this protocol. Specifically, the first set of pCF and cross-pCF results presented here (Fig. 6) were derived from monitoring nanoparticle intracellular transport in the context of drug delivery and used to identify which nanoparticle shapes escape the barriers inside the cell and ultimately reach the nucleus—the expected site of drug release[1]. The second set of cross-pCF results presented here (Fig. 7) were derived from measuring the accessibility of nuclear condensates in the context of DNA repair and used to delineate the mechanism by which p53-binding protein 1 (53BP1) forms foci at DNA double-strand breaks (DSBs)[31].

Intracellular transport of nanoparticles

In recent work, we used pair correlation microscopy to track the translocation route of differently shaped nanoparticles (micelles, vesicles, rods and worms) across subcellular boundaries and extended this method to cross-pair correlation microscopy as a means of identifying when and where differently shaped nanoparticles loaded with a DNA drug

called 'doxorubicin' released their cargo[1]. In this work, we used the procedure described in this protocol, and Fig. 6 shows representative results that were obtained in live MCF7 cells incubated with Hoechst 33342 (blue fluorescence) and fluorescein-labeled nanoparticles (green fluorescence) (Fig. 6a–o) or Cy5-labeled nanoparticles (red fluorescence) loaded with doxorubicin (green autofluorescence) (Fig. 6o). As can be seen in Fig. 6, the line scan selected across an MCF7 cell for FFS data acquisition (Steps 8–16) and ACF versus pCF analysis (Steps 17–24) traversed the extracellular space, cytoplasm and nucleus (Fig. 6b–d) to enable the mobile nanoparticle concentration gradient (Fig. 6e–h) versus translocation path (Fig. 6i–l) across the plasma membrane and nuclear envelope to be quantified. Collectively, this analysis resulted in a series of molecule numbers and arrival times describing micelle-, vesicle-, rod- and worm-shaped nanoparticle intracellular transport that could be statistically compared (Fig. 6m) and enabled identification of the fact that only nanoparticle shapes with a high aspect ratio (such as rods and worms) accessed the cell nucleus (Fig. 6n). This critical insight revealed by pCF analysis was then used to enhance nanoparticle-based delivery of doxorubicin to the cell nucleus. Specifically, upon functionalization, labeling and loading of worm-shaped nanoparticles with a nuclear localization signal (NLS), Cy5 and auto-fluorescent doxorubicin, respectively, a cross-pCF experiment (Steps 25–33) confirmed that this nanoparticle design (informed by pCF analysis) was effective at enhancing doxorubicin molecule delivery to the cell nucleus (Fig. 6o).

Accessibility of intracellular condensates

In recent work, we used cross-pair correlation microscopy to track how a dimeric DNA repair factor called '53BP1' assembles nuclear condensates at DNA DSBs. We used the procedure described in this protocol, and Fig. 7 shows representative results that were obtained in the DSB inducible via an AsiSI (DIvA) cell system co-transfected with 53BP1 tagged to eGFP (eGFP-53BP1) and mKate2 (mKate2-53BP1) (Fig. 7a). As can be seen in Fig. 7, the line scan selected across a DIvA cell for FFS data acquisition (Steps 25–28) and cross-ACF versus pCF analysis (Steps 29–33) traversed a 53BP1 nuclear condensate (Fig. 7b) to enable the normalized fraction of 53BP1 dimers diffusing on versus off a DSB site to be quantified as a function of arrival time (Fig. 7c–f). Collectively, this analysis resulted in a series of pCF profiles that tracked 53BP1 dimer diffusion (Fig. 7g,h) and revealed that 53BP1 foci form from 53BP1 dimers exhibiting a high transport efficiency when diffusing on and not off a DSB site.

Data availability

The pair correlation microscopy line scan data that were acquired for the purpose of this protocol and presented in Figs. 3 and 4 are available online via GitHub (https://github.com/ehinde/Pair-correlation-microscopy). The pair correlation microscopy line scan data presented in Figs. 6 and 7 from previously published papers[1,31] are available from the corresponding author upon request.

Code availability

The 'Pair correlation microscopy' custom MATLAB code described throughout the protocol that was used to analyze the data presented in Figs. 3 and 4 are available online via GitHub (https://github.com/ehinde/Pair-correlation-microscopy).

Received: 19 October 2023; Accepted: 23 October 2024;
Published online: 06 February 2025

References

1. Hinde, E. et al. Pair correlation microscopy reveals the role of nanoparticle shape in intracellular transport and site of drug release. *Nat. Nanotechnol.* **12**, 81–89 (2017).
2. Digman, M. A. & Gratton, E. Imaging barriers to diffusion by pair correlation functions. *Biophys. J.* **97**, 665–673 (2009).
3. Di Rienzo, C., Cardarelli, F., Di Luca, M., Beltram, F. & Gratton, E. Diffusion tensor analysis by two-dimensional pair correlation of fluorescence fluctuations in cells. *Biophys. J.* **111**, 841–851 (2016).
4. Cardarelli, F. & Gratton, E. In vivo imaging of single-molecule translocation through nuclear pore complexes by pair correlation functions. *PLoS One* **5**, e10475 (2010).

5. Hinde, E., Cardarelli, F., Digman, M. A. & Gratton, E. In vivo pair correlation analysis of EGFP intranuclear diffusion reveals DNA-dependent molecular flow. *Proc. Natl Acad. Sci. USA* **107**, 16560–16565 (2010).
6. Malacrida, L., Hedde, P. N., Ranjit, S., Cardarelli, F. & Gratton, E. Visualization of barriers and obstacles to molecular diffusion in live cells by spatial pair-cross-correlation in two dimensions. *Biomed. Opt. Express* **9**, 303–321 (2018).
7. Baum, M., Erdel, F., Wachsmuth, M. & Rippe, K. Retrieving the intracellular topology from multi-scale protein mobility mapping in living cells. *Nat. Commun.* **5**, 4494 (2014).
8. Cardarelli, F., Lanzano, L. & Gratton, E. Capturing directed molecular motion in the nuclear pore complex of live cells. *Proc. Natl Acad. Sci. USA* **109**, 9863–9868 (2012).
9. Gabriel, M. V. et al. Dengue virus capsid-protein dynamics in live infected cells studied by pair correlation analysis. *Methods Mol. Biol.* **2409**, 99–117 (2022).
10. Sallaberry, I. et al. In vivo pair correlation microscopy reveals dengue virus capsid protein nucleocytoplasmic bidirectional movement in mammalian infected cells. *Sci. Rep.* **11**, 24415 (2021).
11. Chiu, C. L., Digman, M. A. & Gratton, E. Measuring actin flow in 3D cell protrusions. *Biophys. J.* **105**, 1746–1755 (2013).
12. Hinde, E., Cardarelli, F., Digman, M. A. & Gratton, E. Changes in chromatin compaction during the cell cycle revealed by micrometer-scale measurement of molecular flow in the nucleus. *Biophys. J.* **102**, 691–697 (2012).
13. Hinde, E. et al. The impact of mitotic versus interphase chromatin architecture on the molecular flow of EGFP by pair correlation analysis. *Biophys. J.* **100**, 1829–1836 (2011).
14. Hinde, E., Cardarelli, F. & Gratton, E. Spatiotemporal regulation of Heterochromatin Protein 1-alpha oligomerization and dynamics in live cells. *Sci. Rep.* **5**, 12001 (2015).
15. Hinde, E., Digman, M. A., Hahn, K. M. & Gratton, E. Millisecond spatiotemporal dynamics of FRET biosensors by the pair correlation function and the phasor approach to FLIM. *Proc. Natl Acad. Sci. USA* **110**, 135–140 (2013).
16. Hinde, E., Kong, X., Yokomori, K. & Gratton, E. Chromatin dynamics during DNA repair revealed by pair correlation analysis of molecular flow in the nucleus. *Biophys. J.* **107**, 55–65 (2014).
17. Mitrentsi, I. et al. Heterochromatic repeat clustering imposes a physical barrier on homologous recombination to prevent chromosomal translocations. *Mol. Cell* **82**, 2132–2147 e2136 (2022).
18. Magde, D., Elson, E. & Webb, W. W. Thermodynamic fluctuations in a reacting system—measurement by fluorescence correlation spectroscopy. *Phys. Rev. Lett.* **29**, 705–708 (1972).
19. Elson, E. L. & Magde, D. Fluorescence correlation spectroscopy. I. Conceptual basis and theory. *Biopolymers* **13**, 1–27 (1974).
20. Magde, D., Elson, E. L. & Webb, W. W. Fluorescence correlation spectroscopy. II. An experimental realization. *Biopolymers* **13**, 29–61 (1974).
21. Ehrenberg, M. & Rigler, R. Rotational Brownian motion and fluorescence intensify fluctuations. *Chem. Phys.* **4**, 390–401 (1974).
22. Ehrenberg, M. & Rigler, R. Fluorescence correlation spectroscopy applied to rotational diffusion of macromolecules. *Q. Rev. Biophys.* **9**, 69–81 (1976).
23. Ruan, Q., Cheng, M. A., Levi, M., Gratton, E. & Mantulin, W. W. Spatial-temporal studies of membrane dynamics: scanning fluorescence correlation spectroscopy (SFCS). *Biophys. J.* **87**, 1260–1267 (2004).
24. Ries, J. & Schwille, P. Studying slow membrane dynamics with continuous wave scanning fluorescence correlation spectroscopy. *Biophys. J.* **91**, 1915–1924 (2006).
25. Ries, J., Chiantia, S. & Schwille, P. Accurate determination of membrane dynamics with line-scan FCS. *Biophys. J.* **96**, 1999–2008 (2009).
26. Ries, J., Yu, S. R., Burkhardt, M., Brand, M. & Schwille, P. Modular scanning FCS quantifies receptor-ligand interactions in living multicellular organisms. *Nat. Methods* **6**, 643–645 (2009).
27. Berland, K. M., So, P. T., Chen, Y., Mantulin, W. W. & Gratton, E. Scanning two-photon fluctuation correlation spectroscopy: particle counting measurements for detection of molecular aggregation. *Biophys. J.* **71**, 410–420 (1996).
28. Dertinger, T. et al. The optics and performance of dual-focus fluorescence correlation spectroscopy. *Opt. Express* **16**, 14353–14368 (2008).
29. Dertinger, T. et al. Two-focus fluorescence correlation spectroscopy: a new tool for accurate and absolute diffusion measurements. *ChemPhysChem* **8**, 433–443 (2007).
30. Wohland, T., Maiti, S. & Macháň, R. *An Introduction to Fluorescence Correlation Spectroscopy* (IOP Publishing, 2020).
31. Lou, J., Priest, D. G., Solano, A., Kerjouan, A. & Hinde, E. Spatiotemporal dynamics of 53BP1 dimer recruitment to a DNA double strand break. *Nat. Commun.* **11**, 5776 (2020).
32. Di Rienzo, C., Gratton, E., Beltram, F. & Cardarelli, F. Spatiotemporal fluctuation analysis: a powerful tool for the future nanoscopy of molecular processes. *Biophys. J.* **111**, 679–685 (2016).
33. Digman, M. A. & Gratton, E. Lessons in fluctuation correlation spectroscopy. *Annu. Rev. Phys. Chem.* **62**, 645–668 (2011).
34. Hinde, E. & Cardarelli, F. Measuring the flow of molecules in cells. *Biophys. Rev.* **3**, 119 (2011).
35. Priest, D. G., Solano, A., Lou, J. & Hinde, E. Fluorescence fluctuation spectroscopy: an invaluable microscopy tool for uncovering the biophysical rules for navigating the nuclear landscape. *Biochem. Soc. Trans.* **47**, 1117–1129 (2019).
36. Hedde, P. N., Staaf, E., Singh, S. B., Johansson, S. & Gratton, E. Pair correlation analysis maps the dynamic two-dimensional organization of natural killer cell receptors at the synapse. *ACS Nano* **13**, 14274–14282 (2019).
37. Bianchini, P., Cardarelli, F., Di Luca, M., Diaspro, A. & Bizzarri, R. Nanoscale protein diffusion by STED-based pair correlation analysis. *PLoS One* **9**, e99619 (2014).
38. Hinde, E. et al. Quantifying the dynamics of the oligomeric transcription factor STAT3 by pair correlation of molecular brightness. *Nat. Commun.* **7**, 11047 (2016).
39. Solano, A., Lou, J., Scipioni, L., Gratton, E. & Hinde, E. Radial pair correlation of molecular brightness fluctuations maps protein diffusion as a function of oligomeric state within live-cell nuclear architecture. *Biophys. J.* **121**, 2152–2167 (2022).
40. Wohland, T., Shi, X., Sankaran, J. & Stelzer, E. H. Single plane illumination fluorescence correlation spectroscopy (SPIM-FCS) probes inhomogeneous three-dimensional environments. *Opt. Express* **18**, 10627–10641 (2010).
41. Krieger, J. W., Singh, A. P., Garbe, C. S., Wohland, T. & Langowski, J. Dual-color fluorescence cross-correlation spectroscopy on a single plane illumination microscope (SPIM-FCCS). *Opt. Express* **22**, 2358–2375 (2014).
42. Krieger, J. W. et al. Imaging fluorescence (cross-) correlation spectroscopy in live cells and organisms. *Nat. Protoc.* **10**, 1948–1974 (2015).
43. Sankaran, J., Bag, N., Kraut, R. S. & Wohland, T. Accuracy and precision in camera-based fluorescence correlation spectroscopy measurements. *Anal. Chem.* **85**, 3948–3954 (2013).
44. Born, M. & Wolf, E. *Principles of Optics: Electromagnetic Theory of Propagation, Interference and Diffraction of Light* 7th edn (Cambridge Univ. Press, 1999).
45. Pawley, J. *Handbook of Biological Confocal Microscopy* (Springer US, 2013).
46. Buschmann, V., Krämer, B., Koberling, F., Macdonald, R. & Rüttinger, S. Quantitative FCS: determination of the confocal volume by FCS and bead scanning with MicroTime 200. *PicoQuant* https://www.picoquant.com/images/uploads/page/files/7351/appnote_quantfcs.pdf (2009).
47. Nagy, A., Wu, J. & Berland, K. M. Characterizing observation volumes and the role of excitation saturation in one-photon fluorescence fluctuation spectroscopy. *J. Biomed. Opt.* **10**, 44015 (2005).
48. Wohland, T., Rigler, R. & Vogel, H. The standard deviation in fluorescence correlation spectroscopy. *Biophys. J.* **80**, 2987–2999 (2001).
49. Bacia, K. & Schwille, P. Practical guidelines for dual-color fluorescence cross-correlation spectroscopy. *Nat. Protoc.* **2**, 2842–2856 (2007).
50. Garcia, D. A. et al. An intrinsically disordered region-mediated confinement state contributes to the dynamics and function of transcription factors. *Mol. Cell* **81**, 1484–1498 e1486 (2021).
51. Hendrix, J. et al. Live-cell observation of cytosolic HIV-1 assembly onset reveals RNA-interacting Gag oligomers. *J. Cell Biol.* **210**, 629–646 (2015).
52. Li, H., Zheng, K., Yang, J. & Zhao, J. Anomalous diffusion inside soft colloidal suspensions investigated by variable length scale fluorescence correlation spectroscopy. *ACS Omega* **5**, 11123–11130 (2020).
53. Culbertson, C. T., Jacobson, S. C. & Michael Ramsey, J. Diffusion coefficient measurements in microfluidic devices. *Talanta* **56**, 365–373 (2002).
54. Gendron, P. O., Avaltroni, F. & Wilkinson, K. J. Diffusion coefficients of several rhodamine derivatives as determined by pulsed field gradient-nuclear magnetic resonance and fluorescence correlation spectroscopy. *J. Fluoresc.* **18**, 1093–1101 (2008).
55. Müller, C. B. et al. Precise measurement of diffusion by multi-color dual-focus fluorescence correlation spectroscopy. *Europhys. Lett.* **83**, 46001 (2008).
56. Rani, S. A., Pitts, B. & Stewart, P. S. Rapid diffusion of fluorescent tracers into *Staphylococcus epidermidis* biofilms visualized by time lapse microscopy. *Antimicrob. Agents Chemother.* **49**, 728–732 (2005).
57. Petrásek, Z. & Schwille, P. Precise measurement of diffusion coefficients using scanning fluorescence correlation spectroscopy. *Biophys. J.* **94**, 1437–1448 (2008).
58. Paul, P. H., Garguilo, M. G. & Rakestraw, D. J. Imaging of pressure- and electrokinetically driven flows through open capillaries. *Anal. Chem.* **70**, 2459–2467 (1998).
59. Potma, E. O. et al. Reduced protein diffusion rate by cytoskeleton in vegetative and polarized *Dictyostelium* cells. *Biophys. J.* **81**, 2010–2019 (2001).
60. Vamosi, G. et al. EGFP oligomers as natural fluorescence and hydrodynamic standards. *Sci. Rep.* **6**, 33022 (2016).
61. Bancaud, A. et al. Molecular crowding affects diffusion and binding of nuclear proteins in heterochromatin and reveals the fractal organization of chromatin. *EMBO J.* **28**, 3785–3798 (2009).
62. Lange, J. J. et al. Correction of bleaching artifacts in high content fluorescence correlation spectroscopy (HCS-FCS) data. In *Proc. SPIE 8590, Single Molecule Spectroscopy and Superresolution Imaging VI* (eds Enderlein, J. et al.) https://doi.org/10.1117/12.2005205 (SPIE, 2013).
63. Di Rienzo, C., Gratton, E., Beltram, F. & Cardarelli, F. Fast spatiotemporal correlation spectroscopy to determine protein lateral diffusion laws in live cell membranes. *Proc. Natl Acad. Sci. USA* **110**, 12307–12312 (2013).
64. Kusumi, A., Sako, Y. & Yamamoto, M. Confined lateral diffusion of membrane receptors as studied by single particle tracking (nanovid microscopy). Effects of calcium-induced differentiation in cultured epithelial cells. *Biophys. J.* **65**, 2021–2040 (1993).
65. Wieser, S. & Schutz, G. J. Tracking single molecules in the live cell plasma membrane—Do's and Don't's. *Methods* **46**, 131–140 (2008).

Acknowledgements

E.H. acknowledges support from the Australian Research Council (ARC) Centre of Excellence in Quantum Biotechnology (CE230100021), an ARC Future Fellowship (FT200100401), ARC Discovery Projects (DP180101387 and DP210102984), an ARC Linkage Infrastructure, Equipment and Facilities (LIEF) Project (LE210100046) and the Jacob Haimson Beverly

Mecklenburg Lectureship. F.C. acknowledges support from the European Research Council (ERC) under the European Union's Horizon 2020 Research and Innovation Program (Grant Agreement No. 866127, project CAPTUR3D). M.A.D acknowledges support from the Paul G. Allen Frontiers Group and National Science Foundation (NSF) (CAREER 1847005).

Author contributions

E.H., F.C., M.A.D. and E.G. conceived the project. J.S.-V., A.S. and E.H. designed the experimental protocol and developed the software. J.S.-V. performed the experiments, analyzed the data and prepared the figures. All authors contributed to the writing of the paper.

Competing interests

The authors declare no competing interests.

Additional information

Supplementary information The online version contains supplementary material available at https://doi.org/10.1038/s41596-024-01097-6.

Correspondence and requests for materials should be addressed to Elizabeth Hinde.

Peer review information *Nature Protocols* thanks Christian Eggeling and the other, anonymous, reviewers for their contribution to the peer review of this work.